



# Depositional Paleoenvironments and Implications on the Occurrence of the Shahejie Formation Source Rock in the Langgu Sag, Bohai Bay Basin

Yijun Cao<sup>1,2</sup>, Fan Diao<sup>3</sup> and Huayao Zou<sup>1,2\*</sup>

<sup>1</sup>State Key Laboratory of Petroleum Resources and Prospecting, China University of Petroleum (Beijing), Beijing, China, <sup>2</sup>College of Geosciences, China University of Petroleum (Beijing), Beijing, China, <sup>3</sup>East China Institute of Technology, Nanchang, China

## OPEN ACCESS

### Edited by:

Bo Liu,  
Northeast Petroleum University, China

### Reviewed by:

Huyue Song,  
China University of Geosciences,  
China  
Quanzhong Guan,  
Chengdu University of Technology,  
China

### \*Correspondence:

Huayao Zou  
mailto:huayaozou@cup.edu.cn

### Specialty section:

This article was submitted to  
Geochemistry,  
a section of the journal  
Frontiers in Earth Science

**Received:** 17 April 2022

**Accepted:** 09 May 2022

**Published:** 15 June 2022

### Citation:

Cao Y, Diao F and Zou H (2022)  
Depositional Paleoenvironments and  
Implications on the Occurrence of the  
Shahejie Formation Source Rock in the  
Langgu Sag, Bohai Bay Basin.  
Front. Earth Sci. 10:922338.  
doi: 10.3389/feart.2022.922338

The fourth (Es<sub>4</sub>) and the third (Es<sub>3</sub>) members of the Eocene Shahejie Formation (Es) are potential source rock intervals in the Langgu hydrocarbon-generating sag. However, the mechanism of source rock occurrence remains poorly understood. In this study, 50 core samples of the Es (21 of Es<sub>4</sub> and 29 of Es<sub>3</sub>) from the Langgu sag were conducted on total organic carbon (TOC) determination, Rock-Eval pyrolysis, carbon isotope of organic matter ( $\delta^{13}\text{C}_{\text{OM}}$ ), carbon ( $\delta^{13}\text{C}_{\text{Carb}}$ ) and oxygen ( $\delta^{18}\text{O}_{\text{Carb}}$ ) isotope of carbonate, bulk mineral compositions, and major and trace element concentrations to characterize the depositional environments and reveal the controlling factors of organic matter enrichment during the deposition of the Es source rock intervals. The Es<sub>4</sub> was deposited in a relatively hydrologically closed saline lake in an arid climate. In comparison, semihumid to humid paleolimnological conditions prevailed during the deposition of Es<sub>3</sub>, which was accompanied by enhanced chemical weathering and relatively low paleosalinity. Redox proxies indicate that the Es<sub>4</sub> rock was deposited in a relatively stronger reducing environment compared to the Es<sub>3</sub>. The relatively high <sup>13</sup>C enrichment in the organic matter ( $\delta^{13}\text{C}_{\text{OM}}$  is as high as  $-23\%$ ) of the Es<sub>3</sub> rock is mainly associated with promoted primary productivity triggered by an increased input/recycling of nutrients favored by semihumid climate and hydrologically open paleolake conditions. The hydrogen index (HI) versus  $\Delta\delta^{13}\text{C}_{\text{Carb-OM}}$  (the difference between the  $\delta^{13}\text{C}_{\text{Carb}}$  and  $\delta^{13}\text{C}_{\text{OM}}$ ) indicates that enhanced preservation and promoted primary productivity seemed to be the main factors in the accumulation of organic matter during the deposition of Es<sub>4</sub> and Es<sub>3</sub> in the Langgu sag, respectively. Nevertheless, the low to medium hydrocarbon-generating potential for Es mudstone indicates that dilution played a significant role in the formation of high-quality source rock apart from the influences of productivity and preservation. In comparison, the limited petroleum potential of Es source rock could be attributed to dilution associated with high sedimentation rate.

**Keywords:** productivity, preservation, dilution, lacustrine source rock, Langgu sag

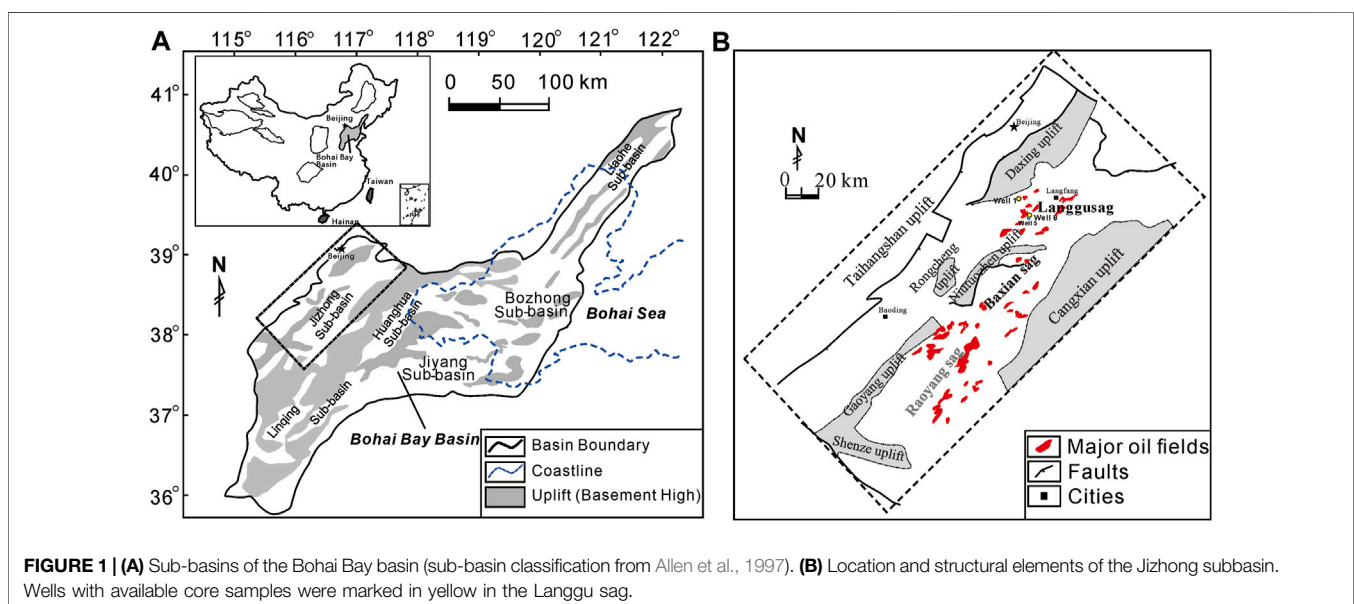
## INTRODUCTION

Lacustrine mud and/or shale rock have been demonstrated to be important source rocks in the worldwide continental rift basins, especially in the areas of China, Indonesia and Brazil with lake facies source rocks as oil and gas sources (Hanson et al., 2001; Gonçalves, 2002; Harris et al., 2004; Wang et al., 2010; Hao et al., 2011; Yin et al., 2020). Previous studies pertaining to lacustrine source rocks deposited in the rift systems revealed that high-quality source rock should be mainly influenced by high productivity and enhanced preservation conditions (Hollander et al., 1993; Katz, 2001; Gonçalves, 2002; Yin et al., 2018). In addition, dilution associated with sedimentation rates also affects the organic matter enrichment (Ibach, 1982; Katz, 2001; Tyson, 2001). However, due to differences in tectonic subsidence and climate, the distribution and characteristics of source rock may reflect interrelated or interacting controls of productivity, preservation, and dilution (Katz, 2005). Therefore, it is necessary to research the paleoclimate conditions and lake environments of source rocks in a specific sedimentary basin (Harris et al., 2004), which may be beneficial for the understanding of the heterogeneous distribution of lacustrine source rocks.

Compared with marine sediments, lacustrine source rocks were deposited under variable paleoenvironments due to the relatively small size of the water reservoir (Hollander and McKenzie, 1991; Valero Garcés et al., 1995). During the last few decades, geochemical characteristics of biomarkers, carbon and oxygen isotopes, minerals and elemental compositions have become effective proxies to illustrate the source input and sedimentary environments (Sinninghe et al., 1995; Meyers, 1997; Harris, 2000; Lamb et al., 2006; Cao et al., 2012; Liu et al., 2017; Wang P. et al., 2020; Wei and Algeo, 2020; Yin et al., 2020). This allows the reconstruction of paleolimnological conditions (e.g., paleoclimate, salinity, etc.) by presenting an

organic and inorganic study of ancient lacustrine sequences to study the formation mechanism of lacustrine source rocks under different tectonic and climatic conditions (Talbot, 1990; Harris, 2000).

A lot of large fields were determined to be sourced from the Es source rocks in the Bohai Bay Basin (BBB) (Hao et al., 2009c; Hao et al., 2010; Hao et al., 2011; Wang et al., 2015; Zhao et al., 2015b; Cao et al., 2017; Zhao et al., 2017). Constricted by coupling effects of structural subsidence and paleoclimate, lacustrine source rocks in a rift basin generally share different petroleum potential with various assemblages of organic facies (Carroll and Bohacs, 1999; Carroll and Bohacs, 2001; Harris et al., 2004; Keym et al., 2006). There exist three hydrocarbon-generating sags, namely, Langgu, Baxian and Raoyang sags, in the Jizhong subbasin, with most of the proved oil reserves being distributed in the vicinity of hydrocarbon-generating sags (Figure 1B). Moreover, differences occur in petroleum resource abundance among these sags (Yin et al., 2018), and the Langgu sag accounts for approximately 10% of the total proved oil reserves in the Jizhong subbasin (Cao et al., 2017; Yin et al., 2018). It is generally believed that the occurrence of high-quality source rocks plays an important role in non-marine petroleum differential enrichment (Hou et al., 2008; Hao et al., 2009a, Hao et al., 2010; Liu et al., 2014). Previous studies have revealed the controlling factors of the Es<sub>1</sub> high-quality source rock interval in the Raoyang and Baxian sags (e.g., Yin et al., 2018). However, few studies have been carried out on the occurrence of Es (i.e., Es<sub>4</sub> and Es<sub>3</sub>) source rock in the Langgu and its related paleolimnological environments. Moreover, the Es source rock in the Langgu sag generally displays relatively lower petroleum potential compared with source rocks in the Raoyang and Baxian sags (Diao et al., 2014). As a result, a systematic geochemical study of Es source rock intervals in the Langgu sag is required to reconstruct the environments and demonstrate the mechanism of organic matter enrichment.



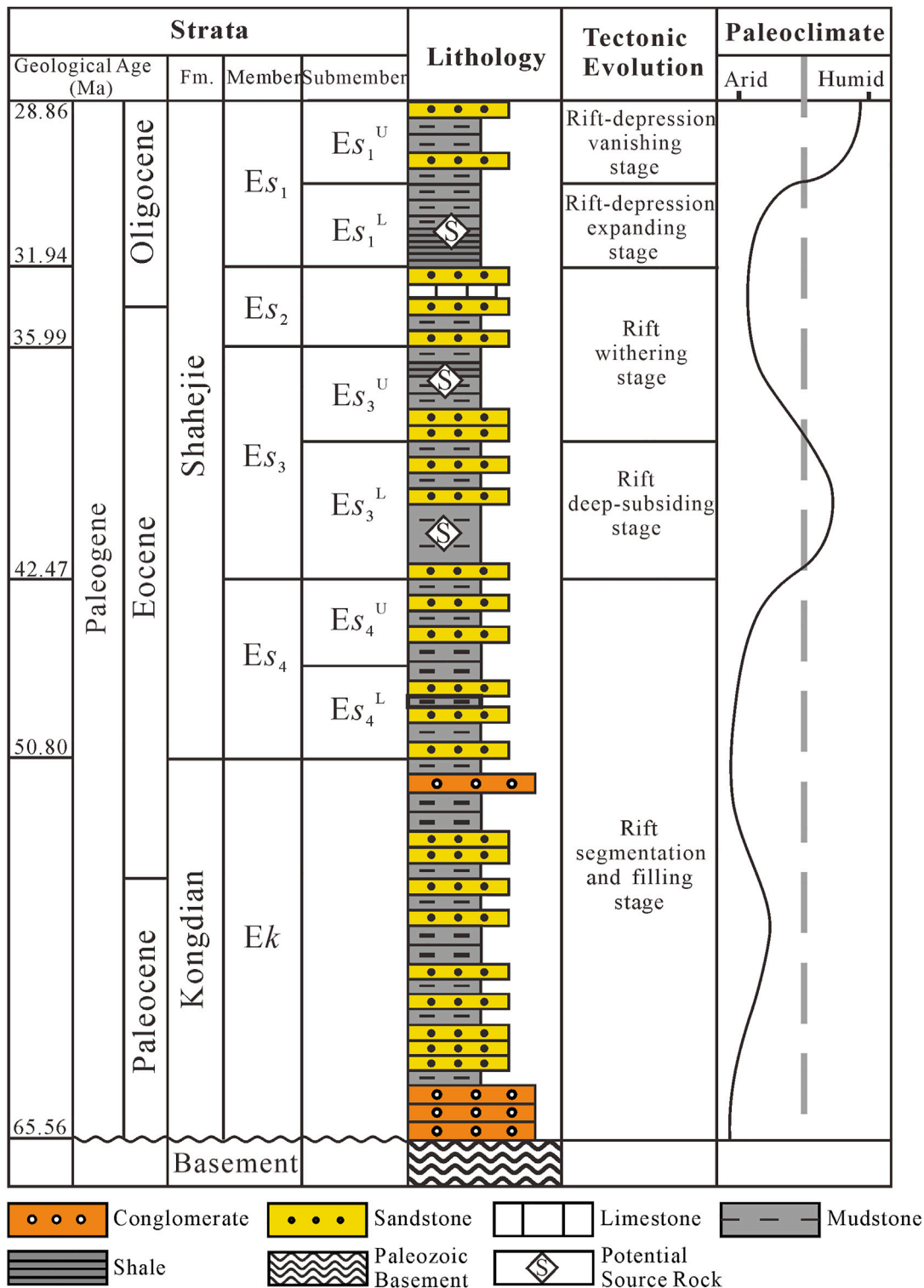


**FIGURE 2** | Generalized stratigraphy of the Paleogene sequences in the Langgu Sag, Jizhong subbasin [modified after Cao et al. (2017)]. The cited ages and the palaeoclimate curve refer to Yin et al. (2018). Potential source rock intervals are marked. Fm, Formation; DY, Dongying; KD, Kongdian.

Two typical wells (well 1 and well 8) drilled Es<sub>3</sub> and Es<sub>4</sub> intervals (**Figure 1B**) with available black mudstone core samples, which provides us an opportunity to present a coupled organic and inorganic geochemical study of potential source rocks in the Langgu sag. The objectives of this study are to characterize the paleolake conditions during source rocks' deposition and to illustrate the organic matter enrichment mechanism of low-abundance lake source rocks under different tectonic and climatic backgrounds. This fundamental research may be helpful for identifying the heterogeneities of non-marine source rock occurrences.

## GEOLOGICAL BACKGROUND

The BBB is a Cenozoic petroliferous lacustrine basin formed on the eastern coast of China with an area of approximately 200,000 km<sup>2</sup>. The BBB generally experienced two major tectonic stages (Allen et al., 1997; Qi and Yang, 2010; Hao et al., 2011; Zhao et al., 2015a) (**Figure 2**), namely, a synrift stage (65–24.6 Ma) consisting of the Paleogene sediments and a postrift stage (24.6 Ma to the present) composed of the Neogene sediments (Hao et al., 2011). The Bohai Bay Basin contains several subbasins; they are Bozhong, Huanghua, Jiyang, Jizhong, Lingqing, and Liaohe (**Figure 1A**). Paleogene sequences, including Kongdian (Ek), Shahejie (Es), and Dongying (Ed) formations, were proved to be important source rocks intervals in these subbasins. However, these source rock intervals were not simultaneously developed in all subbasins, with Ed source rock mainly occurring in the Bozhong subbasin (e.g., Hao et al., 2011).

The Jizhong subbasin, located in the northwestern part of the BBB with an area of 25,000 km<sup>2</sup> (Zhao et al., 2015a), consists of three hydrocarbon-generating sags and several uplifts (**Figure 1A**). The Niutuozhen uplift generally separates the Langgu sag from the Baxian and Raoyang sags (**Figure 1B**). The Eocene Shahejie Formation could be divided into four members, namely, the first member (Es<sub>1</sub>), the second member (Es<sub>2</sub>), the third member (Es<sub>3</sub>), and the fourth member (Es<sub>4</sub>) of the Shahejie Formation (**Figure 2**). Controlled by paleoclimate and structural subsidence (Hao et al., 2011; Zhao et al., 2015b), and potential source rock intervals varied between different sags in the Jizhong subbasin (Diao et al., 2014; Yin et al., 2018). The Es<sub>3</sub> and Es<sub>4</sub> are potential source rock intervals in the Langgu sag (Diao et al., 2014; Cao et al., 2017), whereas the Es<sub>1</sub> is the main source rock in the Baxian and Raoyang sags (Yin et al., 2018). The Langgu sag is bounded by the Daxing boundary fault, which controlled the deposition and evolution of this sag. The Langgu sag generally experienced an initial rift segmentation-filling stage (Ek–Es<sub>4</sub>), rift spreading and deep-subsiding stage (Es<sub>3</sub>), and the rift-depression and vanishing stage (Late Es<sub>3</sub>–Ed) (**Figure 2**) (Zhang et al., 2008; Yin et al., 2018), with a maximum thickness of Paleogene strata up to 9 km (Diao et al., 2014). During the rift segmentation-filling stage, the Langgu sag was the depositional center of the Jizhong subbasin and accumulated thick Es<sub>4</sub> strata with a thickness varying from 400 to 1,600 m. During the deposition of Es<sub>3</sub>, the strong activity of the Daxing

boundary fault resulted in the rapid subsidence of the basement and a wider range of lake water, which resulted in the universal distribution of Es<sub>3</sub> source rock in the Langgu (Song et al., 2006; Zhang et al., 2008). The depocenter had been shifted to the Raoyang and Baxian sags in the Jizhong subbasin during the lift-depression and vanishing stage, which resulted in the universality of high-quality Es<sub>1</sub> source rock in the Baxian and Raoyang sags (Yin et al., 2018). In contrast, the Es<sub>3</sub> and Es<sub>4</sub> mudstones are accepted as the main source rock intervals in the Langgu sag (e.g., Cao et al., 2017).

## SAMPLES AND METHODS

Fifty core samples of the Es (Es<sub>3</sub> and Es<sub>4</sub> samples are from well 1 and well 8, respectively) were collected from exploration wells in the Langgu sag (**Table 1**). To minimize the impact of diagenesis, the pure dark gray mudstone samples without veins were carefully sampled. All the rock samples are cleaned and crushed into powder prior to the experiments. Parallel geochemical experiments, including total organic carbon content (TOC) determination, rock-*eval* pyrolysis, X-ray diffraction (XRD) analyses, isotopic analyses, and major and trace element analyses, are undertaken in this study.

For TOC determination, about 100 mg of rock powder is treated with hydrochloric acid to remove inorganic carbon in carbonates, and then the acid treated sample is saturated with distilled water to a neutral state and dried for 24 h. TOC analysis is completed under the LECO CS230 carbon sulfur analyzer. Rock-Eval pyrolysis is carried out using the Rock-Eval OGE-II instrument. These two kinds of analyses are undertaken in the Petroleum Geology Laboratory, China University of Petroleum (Beijing).

For stable isotope analyses, a split of each source rock sample is decalcified by HCl and combusted at 875°C to generate carbon dioxide (CO<sub>2</sub>) and determine the carbon isotopic compositions of the organic fraction ( $\delta^{13}\text{C}_{\text{OM}}$ ) on a Finnigan MAT 253 mass spectrometer. To obtain the carbon and oxygen isotope ratios of carbonates ( $\delta^{13}\text{C}_{\text{Carb}}$  and  $\delta^{18}\text{O}_{\text{Carb}}$ ), splits of these rock samples are pretreated with H<sub>2</sub>O<sub>2</sub> to eliminate the influence of organics. Then pretreated samples are treated with phosphoric acid at 70°C for at least 3 h to release CO<sub>2</sub>. The analysis of collected CO<sub>2</sub> is performed on a Finnigan MAT 253 mass spectrometer, and the isotopic results are reported in  $\delta^{13}\text{C}$  and  $\delta^{18}\text{O}$  in units of per mil (‰) relative to the international Vienna Pee Dee Belemnite (VPDB) standard. The analytical precision of the  $\delta^{13}\text{C}$  and  $\delta^{18}\text{O}$  values is within 0.1‰.

For trace element analysis, mudstone rock samples are reacted with HNO<sub>3</sub>/HF (1:2) and heated at a temperature of 185°C for 24 h. Detailed procedures are described in Yin et al. (2020). The measurement of trace elements is completed with an inductively coupled plasma-mass spectrometer (ICP-MS; Element XR, Thermo Fisher Scientific Company) with a temperature of 22.6°C and a relative humidity of 43%. The analytical precision is better than 3%. For determination of major element contents, the samples are dissolved with Li<sub>2</sub>B<sub>4</sub>O<sub>7</sub>, NH<sub>4</sub>NO<sub>3</sub>, and LiF and measured by a wavelength dispersive

**TABLE 1** | Basic sample information and measured TOC, HI, isotopic compositions, some major element concentrations, and proxies utilized in this study.

Fm	Depth (m)	TOC (%)	HI	$\delta^{13}\text{C}_{\text{OM}}$	$\delta^{13}\text{C}_{\text{Carb}}$	$\delta^{18}\text{O}_{\text{Carb}}$	$\Delta\delta^{13}\text{C}_{\text{Carb-OM}}$	Si (%)	Al (%)	Ti (%)	Ba-bio	Si-bio	Q/F	$\text{Al}_2\text{O}_3/\text{TiO}_2$	Na/Ti	CIA	Sr/Ba	C-value	V/Cr	V/Sc	EF <sub>U</sub>	EF <sub>M<sub>o</sub></sub>
Es <sub>3</sub>	3407.5	0.60	175	-24.5	0.5	-8.9	25	43.3	12.0	0.58	308	6.2	6.47	23.6	0.89	57.9	0.34	0.26	1.06	6.95	0.93	2.04
Es <sub>3</sub>	3408.75	1.09	220	-25.3	1.3	-9.1	26.6	42.6	12.4	0.55	347	4.3	6.52	25.6	0.98	61.3	0.33	0.21	0.71	5.14	0.51	1.14
Es <sub>3</sub>	3410.7	0.53	160	-25	1.6	-8.2	26.6	44.4	13.2	0.65	404	3.5	5.10	23.1	1.10	64.3	0.33	0.17	0.85	5.04	0.38	0.87
Es <sub>3</sub>	3411.6	0.81	201	-24.8	0.8	-8.3	25.6	49.5	14.5	0.71	468	4.7	3.91	23.0	1.45	70.5	0.27	0.17	0.78	4.69	0.31	0.87
Es <sub>3</sub>	3553.3	0.69	217	-25.5	0.9	-7.5	26.4	53.7	18.0	0.78	190	-2.1	4.77	26.3	1.11	79.9	0.26	0.20	0.68	3.73	0.33	0.60
Es <sub>3</sub>	3556.8	1.14	190	-23.9	0.4	-7.5	24.3	34.0	8.5	0.42	197	7.7	8.14	22.8	0.65	48.7	0.46	0.44	0.36	4.45	0.79	5.03
Es <sub>3</sub>	3563.38	1.39	242	-24.9	0.2	-8.2	25.1	43.8	12.5	0.60	270	5.0	2.27	23.8	0.79	60.5	0.36	0.20	0.72	4.47	0.47	1.91
Es <sub>3</sub>	3565.5	0.52	153	-24.5	0.6	-8.6	25.1	47.9	15.4	0.69	400	0.2	4.56	25.4	1.30	69.2	0.30	0.18	0.56	4.63	0.33	1.11
Es <sub>3</sub>	3567.8	0.96	209	-23	0.9	-8.4	23.9	41.4	11.2	0.60	274	6.8	9.65	21.2	0.72	55.9	0.42	0.20	0.69	4.58	0.50	1.66
Es <sub>3</sub>	3571.2	2.48	226	-24.2	0.6	-9.1	24.8	41.5	11.5	0.72	232	5.8	4.69	18.1	0.83	59.5	0.39	0.27	0.63	5.47	0.55	2.19
Es <sub>3</sub>	3571.7	2.30	256	-24.1	0.6	-7.7	24.7	43.0	12.5	0.65	200	-4.3	6.63	21.8	0.89	63.4	0.32	0.30	0.55	5.14	0.48	2.37
Es <sub>3</sub>	3571.95	2.17	231	-25.8	1.2	-8.8	27	53.1	13.7	0.63	245	10.6	2.48	24.8	2.48	72.2	0.31	0.23	0.67	5.99	0.47	1.87
Es <sub>3</sub>	3572.4	1.90	287	-25.5	0.6	-9.7	26.1	44.2	11.8	0.56	292	7.6	5.98	23.8	1.05	57.9	0.40	0.21	0.63	5.15	0.50	1.89
Es <sub>3</sub>	3572.8	1.87	279	-24.9	0.6	-9.3	25.5	43.0	10.2	0.50	269	11.5	9.17	23.0	0.94	52.6	0.43	0.21	0.58	5.06	0.49	2.20
Es <sub>3</sub>	3573.35	1.23	216	-25.8	0.6	-8.9	26.4	40.6	8.6	0.43	320	14.0	12.04	22.6	0.96	45.4	0.55	0.17	0.56	4.76	0.61	2.71
Es <sub>3</sub>	3573.85	0.78	167	-25.6	1.5	-10.6	27.1	49.5	12.3	0.57	341	11.2	3.73	24.4	2.08	62.7	0.42	0.20	0.52	5.23	0.42	2.04
Es <sub>3</sub>	3574.7	0.74	151	-25.8	3.2	-7.4	29	43.5	11.5	0.60	277	7.9	6.19	21.8	0.80	65.3	0.29	0.29	1.22	7.27	0.73	1.68
Es <sub>3</sub>	3575.6	0.89	99	-25.5	2.7	-9.4	28.2	51.9	13.7	0.63	228	9.4	1.60	24.9	2.11	69.3	0.39	0.22	0.79	7.13	0.48	1.33
Es <sub>3</sub>	3577.43	1.02	191	-27.8	1.7	-8.2	29.5	43.9	12.2	0.60	240	6.0	6.02	23.1	0.94	61.5	0.36	0.23	1.07	6.93	0.49	1.19
Es <sub>3</sub>	3577.9	0.74	219	-27.3	0.3	-8.3	27.6	46.0	11.2	0.51	207	11.3	10.92	24.9	0.93	58.1	0.36	0.23	1.10	7.00	0.75	2.39
Es <sub>3</sub>	3578.93	1.52	243	-27	0.9	-8.6	27.9	37.9	10.8	0.54	187	4.5	9.84	22.6	0.73	54.0	0.36	0.23	0.62	4.97	0.55	1.32
Es <sub>3</sub>	3580.1	0.50	132	-26.4	1.2	-10	27.6	53.4	14.8	0.66	320	7.7	2.56	25.4	2.11	70.8	0.33	0.25	0.66	6.16	0.47	1.83
Es <sub>3</sub>	3620.1	0.84	163	-26.5	0.3	-8.2	26.8	44.2	12.6	0.61	198	5.1	10.66	23.6	0.75	61.9	0.30	0.29	0.72	5.59	0.56	1.65
Es <sub>3</sub>	3621.14	0.59	98	-24.6	0.5	-12.3	25.1	61.6	15.2	0.69	226	14.4	3.28	25.0	2.37	77.0	0.29	0.21	0.67	5.95	0.41	0.88
Es <sub>3</sub>	3621.89	0.76	154	-25.4	1.2	-10	26.6	57.2	14.4	0.66	209	12.7	2.84	24.7	2.37	72.6	0.34	0.24	0.57	5.83	0.41	1.26
Es <sub>3</sub>	3622.7	0.57	141	-25.7	0.7	-8.4	26.4	48.9	15.3	0.71	251	1.6	6.22	24.5	1.15	70.6	0.28	0.19	1.06	6.19	0.43	0.74
Es <sub>3</sub>	3624.73	0.80	172	-25.3	1.8	-9.4	27.1	52.9	15.4	0.71	281	5.2	2.79	24.7	1.89	73.4	0.31	0.22	0.97	6.59	0.43	1.11
Es <sub>3</sub>	3625.7	0.84	146	-25.6	1.2	-8.8	26.8	51.9	14.7	0.68	227	6.3	3.34	24.5	1.78	71.8	0.34	0.21	1.06	6.26	0.45	1.19
Es <sub>3</sub>	3627.4	0.84	158	-25.3	1.7	-9.3	27	54.7	15.0	0.69	259	8.4	2.84	24.5	2.04	72.7	0.33	0.26	0.78	7.39	0.45	1.65
Es <sub>4</sub>	4119.4	0.76	99	-26.8	2.2	-9.9	29	44.9	13.6	0.53	113	2.6	3.84	29.0	1.49	61.2	0.85	0.14	1.24	6.44	0.38	0.52
Es <sub>4</sub>	4120.3	1.85	47	-27.1	3.1	-8.8	30.2	40.9	11.5	0.46	415	5.3	3.48	28.3	1.69	53.3	0.93	0.11	1.27	7.35	0.46	1.12
Es <sub>4</sub>	4121.3	0.73	112	-27.1	3.3	-8.5	30.4	41.1	11.5	0.46	665	5.4	2.92	28.1	1.66	54.4	0.74	0.09	1.64	8.28	0.48	1.03
Es <sub>4</sub>	4122.6	0.91	121	-27.8	3.3	-9.4	31.1	32.3	10.2	0.43	1,566	0.6	2.76	26.9	1.72	42.5	0.49	0.07	1.45	7.63	0.54	1.45
Es <sub>4</sub>	4124	0.97	68	-26.5	2.3	-9.8	28.8	45.4	13.8	0.54	568	2.6	5.69	28.8	1.43	62.3	0.49	0.10	1.50	7.48	0.43	0.49
Es <sub>4</sub>	4124.62	1.16	123	-28.2	3.3	-9.5	31.5	28.8	8.5	0.35	480	2.5	3.80	27.1	1.92	35.8	1.36	0.08	1.46	8.80	0.62	2.02
Es <sub>4</sub>	4125.32	0.86	131	-27.4	2.7	-9.5	30.1	37.1	11.8	0.46	283	0.5	3.99	29.2	1.41	50.7	0.95	0.13	1.77	9.44	0.52	0.68
Es <sub>4</sub>	4125.72	1.22	159	-25.4	3	-9.3	28.4	41.0	11.8	0.51	42	4.5	2.83	26.2	2.00	54.2	1.45	0.16	1.46	9.01	0.77	2.29
Es <sub>4</sub>	4127.42	0.80	158	-25.3	4.8	-6	30.1	34.7	8.0	0.34	96	10.0	4.34	26.3	2.19	42.7	1.56	0.14	1.60	9.96	0.66	2.45
Es <sub>4</sub>	4128.42	0.90	42	-27	5.2	-5.5	32.2	33.5	8.5	0.36	119	7.2	3.68	26.8	2.04	44.7	1.31	0.16	1.53	10.87	0.69	3.01
Es <sub>4</sub>	4130.44	0.71	307	-27.8	3.3	-11	31.1	43.5	10.7	0.45	96	10.2	4.13	27.0	1.96	52.0	2.05	0.11	1.88	10.15	0.60	1.25
Es <sub>4</sub>	4132.59	1.11	185	-28.6	3.1	-9.9	31.7	38.3	11.9	0.45	120	1.6	2.54	30.0	1.57	52.1	1.10	0.17	1.24	8.29	0.51	1.27
Es <sub>4</sub>	4133.44	0.82	186	-28.1	2.7	-10.3	30.8	41.5	13.0	0.51	61	1.2	3.17	28.9	1.65	57.3	0.97	0.16	1.49	7.98	0.49	0.74
Es <sub>4</sub>	4134.8	0.82	196	-28.8	3	-9.7	31.8	36.3	11.6	0.45	147	0.4	3.88	29.5	1.64	49.9	1.36	0.15	1.68	9.90	0.54	1.31
Es <sub>4</sub>	4135.84	0.79	225	-28.9	3.3	-9	32.2	35.1	11.1	0.42	207	0.8	4.36	29.7	1.68	48.2	1.44	0.14	2.00	11.72	0.62	1.90
Es <sub>4</sub>	4184.25	1.66	153	-27.3	3	-10.3	30.3	36.9	9.8	0.44	33	6.4	2.65	25.6	2.60	46.8	2.54	0.14	1.22	10.34	0.69	2.54
Es <sub>4</sub>	4185.8	1.68	161	-27.7	2.6	-10.8	30.3	42.1	12.7	0.51	207	2.7	2.89	28.4	1.89	56.5	1.63	0.15	1.19	10.55	0.67	2.37
Es <sub>4</sub>	4186.9	0.85	77	-27.2	3.4	-8	30.6	27.9	8.8	0.35	281	0.6	2.10	28.3	1.94	43.9	1.27	0.14	1.93	13.38	1.11	3.44
Es <sub>4</sub>	4187.88	1.29	86	-27.1	1.1	-9.8	28.2	50.5	15.6	0.64	-38	2.1	2.34	27.5	1.99	71.7	0.97	0.26	1.43	10.31	0.55	2.63
Es <sub>4</sub>	4188.92	1.77	98	-28.2	1.5	-10.6	29.7	48.8	14.0	0.59	23	5.4	2.61	27.1	2.27	68.6	1.16	0.22	1.63	11.61	0.77	2.34
Es <sub>4</sub>	4190.15	1.27	107	-27.2	2.7	-9.2	29.9	41.7	11.9	0.51	72	4.8	3.14	26.2	2.20	58.5	1.19	0.20	1.33	10.49	0.65	3.11

Fm, Formation; The unit of HI, is mg/g TOC; Q/F, the contents of Quartz to Feldspar; C-value,  $\Sigma(\text{Fe} + \text{Mn} + \text{Cr} + \text{Ni} + \text{V} + \text{Co})/\Sigma(\text{Ca} + \text{Mg} + \text{Sr} + \text{Ba} + \text{K} + \text{Na})$ ; CIA, Chemical index of alteration; CIA (%),  $100 \times \text{Al}_2\text{O}_3/(\text{Al}_2\text{O}_3 + \text{CaO}^* + \text{Na}_2\text{O} + \text{K}_2\text{O})$ , CaO\* represents only CaO in the silicate fraction, and the correction procedure for CaO\* follows that in McLennan (1993). The element concentrations for calculating parameters were provided in Table 2.

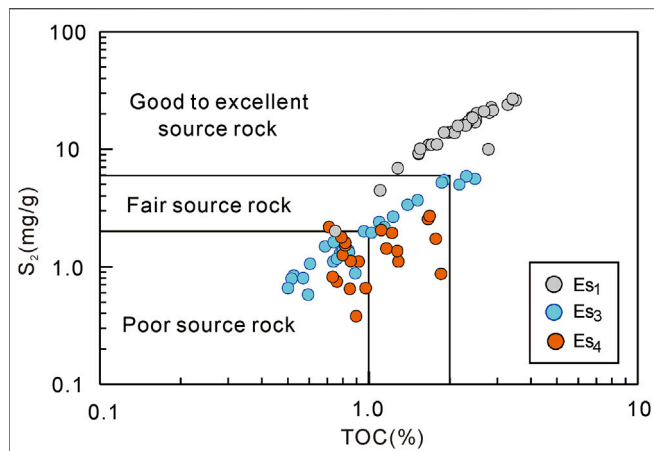


**FIGURE 3** | Crossplot of total organic carbon (TOC) contents vs. Rock-Eval  $S_2$  values for Es rock samples from the Langgu sag, Jizhong subbasin. The classifications refer to Hao et al. (2009b). The  $Es_1$  source rock samples from the Raoyang sag (Yin et al., 2018) were plotted for comparison of hydrocarbon-generating potentials.

X-ray fluorescence spectrometer. The precision and accuracy of results are better than  $\pm 4\%$ .

The remaining powder samples are also selected for XRD analysis to understand bulk mineral compositions. This experiment is carried out on a Bruker D2 PHASER diffractometer system with operating conditions at 30 kV/10 mA, Cu-K $\alpha$  radiation, and a scanning speed of  $2\theta$  2°/min. The total scanning range was 5°–45°(2 $\theta$ ). The stable isotope analyses, major and trace element analyses, and XRD analyses are undertaken at the Beijing Research Institute of Uranium Geology.

## RESULTS

### Rock-Eval Pyrolysis and Total Organic Carbon determination

The TOC, expressed as the weight percent of organic carbon per gram of rock, is an indicator of the total amount of organic matter in sediment. Rock-Eval pyrolysis yields  $S_2$  values (measured in milligrams of hydrocarbons per gram of rock, mg HC/g rock) that represent the amount of hydrocarbons formed during the thermal decomposition of kerogen (Espitalié et al., 1977). In the Langgu sag, the  $Es_4$  source rock has a TOC content ranging from 0.71 to 1.85 wt% (average 1.09 wt%) and  $S_2$  values from 0.38 mg/g rock to 2.7 mg/g rock, with an average value of 1.41 mg/g rock. The  $Es_3$  samples have TOC contents varying from 0.5 to 2.48 wt%, with a mean value of 1.07 wt%, and  $S_2$  values from 0.58 to 5.88 mg HC/g rock, with an average of 2.23 mg HC/g rock (Figure 3 and Table 1). The hydrogen index (HI) was calculated using the formula  $HI = S_2/TOC \times 100$ . HI values for  $Es_4$  samples are reported to vary between 42 and 307 mg HC/g TOC, with an average of 135 mg HC/g TOC. The  $Es_3$  samples have HI values ranging from 98 to 287 mg HC/g TOC, averaging 189 mg HC/g TOC (Table 1).

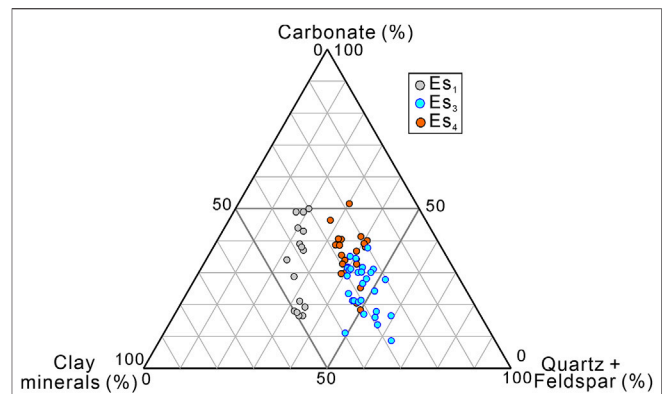


**FIGURE 4** | Ternary diagram of the mineralogy of the  $Es_3$  and  $Es_4$  samples in the Langgu sag. The  $Es_1$  samples from the Raoyang sag were from Yin et al. (2018).

### Mineralogical Composition of Source Rocks

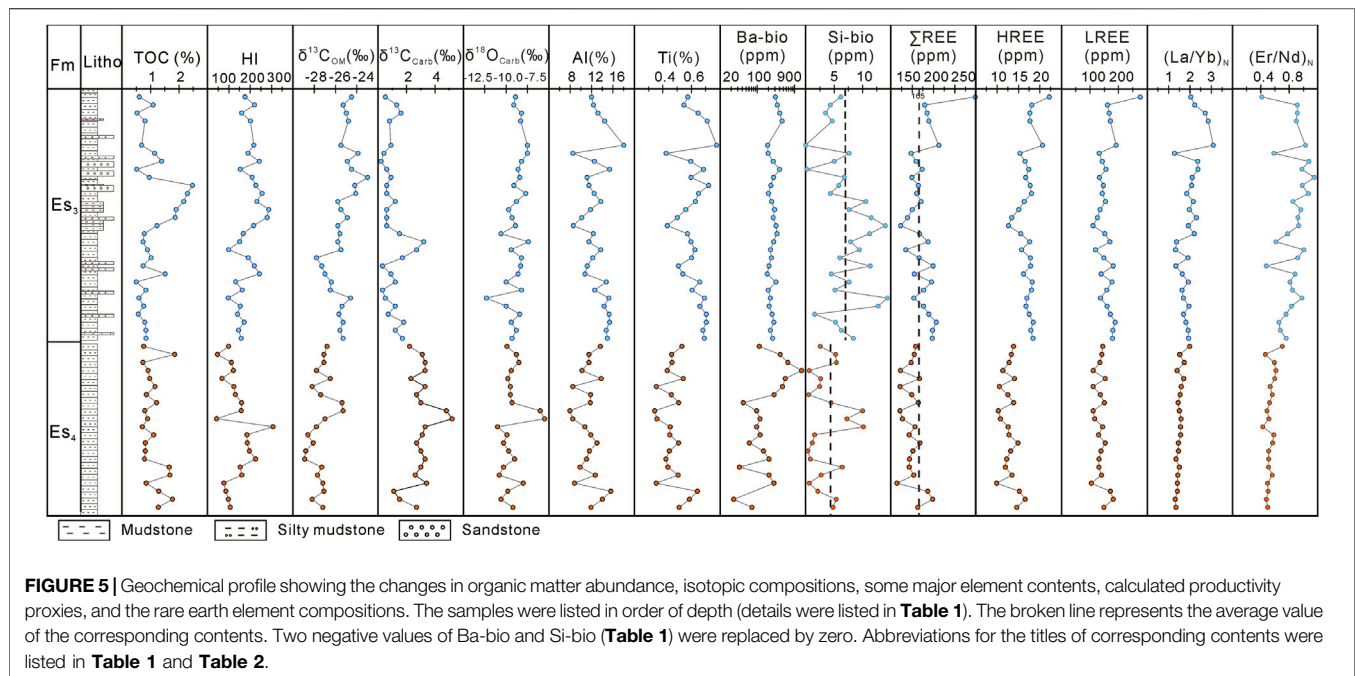
The  $Es_4$  samples generally have higher carbonate content (17.8%–50.9%, averaging 34.9%) than the  $Es_3$  samples (8.6%–36.8%, averaging 24.2%). The  $Es_3$  and  $Es_4$  samples have felsic minerals (quartz + feldspar) contents of 37.7%–62.4% and 26.4%–48.4%, respectively. The latter have relatively focused but lower quartz to feldspar ratios (Q/F) (Table 1). In contrast to the  $Es_1$  source rock in Raoyang sag, the  $Es_3$  and  $Es_4$  samples in the Langgu sag generally contain lower clay contents and higher quartz-feldspar contents (Figure 4).

### Stable Carbon and Isotope Compositions

The  $\delta^{13}C_{\text{Carb}}$  values of the  $Es_3$  samples range from 0.2‰ to 3.2‰ with an average value of 1.0‰. In comparison, the  $Es_4$  samples have relatively  $^{13}C$ -enriched inorganic carbon isotopes, with  $\delta^{13}C_{\text{Carb}}$  ranging from 1.1‰ to 5.2‰ and being mostly greater than 2.0‰ (Figure 5 and Table 1). The  $\delta^{18}O_{\text{Carb}}$  values for  $Es_3$  and  $Es_4$  samples vary from  $-9.9\text{‰}$  to  $-4.5\text{‰}$  and from  $-11\text{‰}$  to  $-5.5\text{‰}$ , respectively. The  $\delta^{18}O_{\text{Carb}}$  values fall in the  $\delta^{18}O_{\text{Carb}}$  range ( $-15\text{‰}$ – $5.5\text{‰}$ ) of non-marine carbonates reported by Drummond et al. (1993). Although most of the  $Es_3$  and  $Es_4$  samples have a similar range of  $\delta^{18}O_{\text{Carb}}$ , the  $Es_4$  samples show a larger variance of  $\delta^{18}O_{\text{Carb}}$  compared to that of the  $Es_3$  (Figure 5 and Table 1). The  $\delta^{13}C_{\text{Omn}}$  for the  $Es_4$  samples varied from  $-28.9\text{‰}$  to  $-25.3\text{‰}$  with a mean value of  $-27.4\text{‰}$ . Compared to the  $Es_4$  samples, the  $Es_3$  samples are relatively enriched in  $^{13}C$  in organic matter and have  $\delta^{13}C_{\text{Omn}}$  values from  $-27.8\text{‰}$  to  $-23.0\text{‰}$ , averaging  $-25.4\text{‰}$  (Table 1).

### Major and Trace Element Compositions

Table 1 and Table 2 show concentrations and the corresponding parameters of the major and trace elements used in this study. The  $Es_4$  samples display strontium/barium (Sr/Ba) values of 0.49–2.54 (mean 1.23), and the  $Es_3$  samples generally display obviously lower Sr/Ba values of 0.26–0.55 (mean 0.35). The sodium/titanium (Na/Ti) ratios for  $Es_3$  and  $Es_4$  samples range from 0.65 to 2.48 and from 1.41 to 2.6,



respectively. Slightly different than  $Es_4$ , the  $Es_3$  samples generally exhibit a broader range but overall lower values of Na/Ti (**Figure 6**). The ratios of aluminum (Al) to Ti (calculated as  $Al_2O_3/TiO_2$  in this study) for  $Es_3$  samples range from 18.1 to 26.3, with an average of 23.7. In comparison, the  $Es_4$  samples have overall higher Al/Ti ratios, varying from 25.6 to 30, with a mean value of 27.9. The calculated values of the chemical index of alteration (CIA) for the  $Es_3$  samples range from 45.4 to 79.9 with a mean value of 64.2. The  $Es_4$  samples display broader but relatively lower CIA values (35.8–71.7, average 52.7) (**Figure 6**). The non-detrital composition of Ba and silicon (Si) elements (expressed as Ba-bio and Si-bio) is calculated by the formula ( $X\text{-bio} = X_{\text{sample}} - Al_{\text{sample}} \times (X/Al)_{\text{detrital}}$ ). Previous studies yielded  $(Ba/Al)_{\text{detrital}}$  values in the range of 0.0032 and 0.0046 (e.g., Schoepfer et al., 2015; Zhou et al., 2015), and a median value (0.0039) of this range was used to represent  $(X/Al)_{\text{detrital}}$  in this study. A suggested Si/Al ratio of 3.1 is used as a detrital value (Wedepohl, 1971) for calculating Si-bio values. The Ba-bio concentration for  $Es_3$  samples ranges from 187 to 468 ppm, with a mean value of 271. The  $Es_4$  samples have relatively scattered but lower Ba-bio values between -38 and 665 ppm, with an abnormally high value of 1,566 (**Figure 5**). The  $Es_3$  and  $Es_4$  samples have Si-bio values varying from -2 to 14 and from 0 to 10, with a mean value of 7 and 4, respectively (**Table 1**). The ratios of vanadium to chromium (V/Cr) and vanadium to scandium (V/Sc) for  $Es_4$  samples range from 1.19 to 2.0 and from 6.43 to 13.38, respectively. Compared to  $Es_4$ , the  $Es_3$  samples have relatively lower ratios of V/Cr (0.36–1.22) and V/Sc (3.73–7.39). Both  $Es_3$  and  $Es_4$  have relatively low ratios of uranium to thorium (U/Th) not exceeding 0.5, with U/Th values ranging from 0.17 to 0.26 (mean 0.21) and from 0.19 to 0.48 (mean 0.26) for  $Es_3$  and  $Es_4$  samples, respectively. The

enrichments of Mo and U in the study were reported by the enrichment factors followed the equation  $[EF_X = (X/Al)_{\text{sample}} / (X/Al)_{\text{PAAS}}]$  raised by (Algeo and Tribovillard, 2009). The  $Es_4$  samples have  $EF_{Mo}$  ratios between 0.49 and 3.44 and  $EF_U$  ratios between 0.38 and 1.11, with a mean value of 1.81 and 0.61, respectively (**Figure 6** and **Table 1**). The  $Es_3$  samples display  $EF_{Mo}$  values of 0.6–5.03 (average 1.68) and  $EF_U$  values of 0.31–0.93 (average 0.51). In addition, most of the analyzed samples (with an exception sample for  $Es_4$ ) show  $EF_U$  values  $< 1.0$ , indicating relative depletion of the element U (Tribovillard et al., 2006).

## Rare Earth Elements

The total content of rare earth elements ( $\Sigma\text{REE}$ ) for  $Es_3$  and  $Es_4$  samples ranges from 123 to 212 ppm, with an exception value of 298 and from 114 to 198 ppm, respectively (**Figure 5** and **Table 3**). The average value of the  $\Sigma\text{REE}$  for all samples was 165 ppm, which was lower than that of the North American Shale Composite (NASC, 173 ppm; Haskin et al., 1968). All REE contents of the Es samples were normalized to the NASC and shown in **Figures 7A,B**. Despite different source intervals, there were no major variations in the REE concentrations, with relatively flat and similar NASC-normalized REE distribution patterns. What is noteworthy is that heavy REE (HREE) in the  $Es_3$  samples shows a relatively rich trend, which is in accordance with the lower ratios (7.6–12.4, average 9.2) of light REE to heavy REE (LREE/HREE). In comparison, the  $Es_4$  samples have relatively higher LREE/HREE ratios between 9.8 and 11.5 (average 10.7). The ratios of normalized lanthanum to ytterbium  $(La/Yb)_N$  (where N represents the concentration normalized to NASC) in the  $Es_3$  and  $Es_4$  samples range from 1.3 to 3.1 (average 2.0) and from 1.3 to 2.0 (average 1.5). The ratios

**TABLE 2** | Some major element concentrations and trace element concentrations of Es<sub>3</sub> and Es<sub>4</sub> mudstone in the Langgu sag.

Fm	Depth (m)	Fe	MgO	CaO	Na	K	MnO	Sc	V	Cr	Co.	Ni	Cu	Zn	Sr	Mo	Cd	Ba	Th	U
		%										ppm (µg/g)								
Es <sub>3</sub>	3407.5	3.66	4.26	13.66	0.51	2.67	0.10	15.4	107	101	25.8	33.4	27	88.2	262	2.91	0.10	776	19.0	3.8
Es <sub>3</sub>	3408.75	5.68	4.04	12.08	0.53	2.6	0.21	16.3	83.8	118	6.14	20.1	70.6	65.4	276	1.67	0.15	829	10.1	2.1
Es <sub>3</sub>	3410.7	5.20	3.99	11.06	0.71	2.69	0.15	15.8	79.6	93.3	6.45	19.5	25.6	59.6	301	1.37	0.17	918	9.6	1.7
Es <sub>3</sub>	3411.6	4.44	3.75	8.12	1.03	2.82	0.08	16.6	77.9	100	13.3	31.8	24.1	68.4	281	1.5	0.19	1032	8.4	1.5
Es <sub>3</sub>	3553.3	4.58	2.85	4.13	0.86	3.84	0.05	20.4	76	111	11	28.5	28.8	70.9	228	1.29	0.19	893	11.5	2.0
Es <sub>3</sub>	3556.8	12.62	4.18	14.81	0.28	2.1	0.09	11.9	53	148	52.5	80.8	20	71.2	244	5.08	0.13	528	9.2	2.3
Es <sub>3</sub>	3563.38	4.36	4.42	12.39	0.47	2.83	0.07	15.2	68	94.2	12.9	28.1	25.8	61.7	271	2.85	0.15	758	9.1	2.0
Es <sub>3</sub>	3565.5	3.81	3.63	9.07	0.89	3.13	0.07	16.1	74.5	133	8.03	23	28.8	70.9	301	2.04	0.21	1000	9.6	1.7
Es <sub>3</sub>	3567.8	5.12	4.59	13.96	0.43	2.65	0.08	15.3	70.1	102	9.49	23	66.9	61.2	301	2.21	0.13	709	8.9	1.9
Es <sub>3</sub>	3571.2	5.06	4.44	12.51	0.60	2.51	0.11	14.8	81	128	13.6	30.9	70.9	80.4	266	3	0.16	681	8.9	2.1
Es <sub>3</sub>	3571.7	5.27	4.95	10.90	0.58	2.75	0.10	14.7	75.6	138	16.8	43.6	29.9	74.3	217	3.52	0.16	687	10.0	2.0
Es <sub>3</sub>	3571.95	4.51	3.19	6.59	1.56	2.44	0.09	13.4	80.3	120	9.99	22.3	24.4	75.9	244	3.06	0.19	780	8.4	2.2
Es <sub>3</sub>	3572.4	3.67	3.71	13.44	0.59	2.54	0.21	13.4	69	109	11.3	28.5	68.4	71.1	299	2.66	0.12	752	8.9	2.0
Es <sub>3</sub>	3572.8	3.66	4.18	14.85	0.47	2.24	0.27	12.1	61.2	105	9.88	22.3	20.9	59.9	289	2.66	0.15	665	7.5	1.7
Es <sub>3</sub>	3573.35	3.60	4.56	17.52	0.41	1.95	0.16	10.7	50.9	91	9.66	25.1	19.9	44.7	361	2.77	0.11	655	7.5	1.8
Es <sub>3</sub>	3573.85	4.39	2.68	10.88	1.19	2.35	0.10	12.8	67	130	11.3	26.4	22	83.3	347	2.99	0.13	822	8.4	1.7
Es <sub>3</sub>	3574.7	10.62	3.76	9.09	0.48	2.64	0.20	17.6	128	105	8.79	19.4	26.3	55.6	213	2.3	0.08	725	12.4	2.8
Es <sub>3</sub>	3575.6	5.80	2.31	8.31	1.32	2.57	0.13	12.3	87.7	111	8.38	20	23.1	97.1	294	2.17	0.19	763	10.3	2.2
Es <sub>3</sub>	3577.43	5.60	3.98	11.97	0.57	2.78	0.14	14.1	97.7	91.5	10.2	24.6	26.8	62.2	256	1.73	0.08	717	9.5	2.0
Es <sub>3</sub>	3577.9	4.26	4.90	12.41	0.47	2.56	0.09	12.8	89.6	81.5	12.4	19.2	23	77.9	229	3.19	0.11	643	12.5	2.9
Es <sub>3</sub>	3578.93	5.03	6.15	14.80	0.39	2.59	0.12	12.7	63.1	102	6.5	17.7	23	45.8	218	1.7	0.08	607	10.4	2.0
Es <sub>3</sub>	3580.1	4.80	2.32	7.42	1.39	2.89	0.07	14.5	89.3	135	22.4	46.6	25.4	73.3	298	3.21	0.18	895	11.4	2.3
Es <sub>3</sub>	3620.1	5.21	4.51	11.60	0.45	2.93	0.12	15.3	85.6	119	21.3	37.7	29.8	76.7	209	2.47	0.17	689	10.9	2.4
Es <sub>3</sub>	3621.14	3.82	1.82	3.90	1.64	2.95	0.06	12.3	73.2	109	10.8	23.6	22.4	101	236	1.6	0.15	820	10.6	2.1
Es <sub>3</sub>	3621.89	3.68	2.32	6.25	1.56	2.66	0.08	13.2	77	135	10.2	26.7	23.1	72.4	258	2.16	0.18	769	9.7	2.0
Es <sub>3</sub>	3622.7	4.47	3.54	8.34	0.81	3.16	0.12	14.7	91	85.8	10.3	20.5	29.1	82.8	237	1.35	0.13	847	12.3	2.2
Es <sub>3</sub>	3624.73	4.54	2.58	6.61	1.33	2.89	0.11	14.9	98.2	101	15.9	32	28.9	101	274	2.03	0.18	880	11.1	2.3
Es <sub>3</sub>	3625.7	4.74	3.16	7.39	1.21	2.76	0.12	14.7	92	87	15.2	31.4	26.2	89.3	270	2.09	0.19	801	10.5	2.2
Es <sub>3</sub>	3627.4	4.27	2.46	6.65	1.41	2.78	0.10	14.2	105	135	14.9	34.6	69.9	87.9	275	2.94	0.17	842	10.5	2.3
Es <sub>4</sub>	4119.4	4.17	2.56	13.52	0.80	2.49	0.12	12.6	81.1	65.4	7.49	16.3	22.3	68.1	546	0.85	0.15	645	9.2	1.7
Es <sub>4</sub>	4120.3	4.21	2.75	17.05	0.78	2.09	0.13	11.3	83	65.6	11	25.8	20	78.8	801	1.54	0.16	863	8.0	1.8
Es <sub>4</sub>	4121.3	4.44	2.90	16.36	0.77	2.02	0.12	10.9	90.2	55	9.75	21.9	17.5	82	823	1.41	0.19	1113	8.2	1.9
Es <sub>4</sub>	4122.6	3.14	2.96	23.56	0.74	2.02	0.09	10.5	80.1	55.3	18.2	43.6	22.9	84.8	956	1.76	0.16	1964	7.7	1.9
Es <sub>4</sub>	4124	4.10	2.56	12.93	0.78	2.56	0.12	12	89.8	59.8	4.25	13.1	21.8	81.8	544	0.81	0.15	1107	10.7	2.0
Es <sub>4</sub>	4124.62	2.82	2.76	27.11	0.68	1.62	0.11	8.19	72.1	49.4	7.66	21.6	16.4	75	1103	2.04	0.13	811	6.3	1.8
Es <sub>4</sub>	4125.32	3.75	2.62	19.41	0.65	2.19	0.14	10.8	102	57.7	10.6	22.3	21.3	70.3	708	0.96	0.13	744	9.2	2.1
Es <sub>4</sub>	4125.72	2.82	3.90	16.14	1.02	2.27	0.07	10.1	91	62.5	15.3	30.7	71.9	90.4	727	3.21	0.16	501	9.4	3.1
Es <sub>4</sub>	4127.42	3.25	7.55	18.52	0.75	1.49	0.07	7.12	70.9	44.4	10.1	16.4	12.2	130	634	2.32	0.14	406	6.4	1.8
Es <sub>4</sub>	4128.42	3.65	7.47	18.11	0.73	1.61	0.07	7.51	81.6	53.4	10.3	23.6	17.3	93.1	587	3.04	0.14	449	6.7	2.0
Es <sub>4</sub>	4130.44	3.64	2.54	17.22	0.88	1.92	0.07	9.35	94.9	50.6	10.1	20.2	17.3	79.6	1055	1.6	0.13	515	8.2	2.2
Es <sub>4</sub>	4132.59	4.04	2.92	18.06	0.70	2.26	0.11	10.5	87	70.2	15	30.7	23.5	138	640	1.79	0.15	582	8.7	2.0
Es <sub>4</sub>	4133.44	4.22	2.64	15.64	0.84	2.43	0.11	11.1	88.6	59.3	10.8	22.2	21.2	126	553	1.15	0.13	569	10.3	2.2
Es <sub>4</sub>	4134.8	3.67	2.89	19.75	0.73	2.22	0.12	10.4	103	61.3	13.9	31.6	23.7	106	817	1.81	0.17	599	8.8	2.1
Es <sub>4</sub>	4135.84	4.05	3.30	20.01	0.71	2.08	0.10	9.56	112	56.1	12.9	31.2	21.2	106	916	2.5	0.16	638	8.7	2.3
Es <sub>4</sub>	4184.25	3.73	3.77	19.03	1.13	1.88	0.08	8.31	85.9	70.4	12	30.7	24.4	115	1061	2.97	0.14	417	7.8	2.3
Es <sub>4</sub>	4185.8	4.06	2.83	15.27	0.96	2.53	0.06	10.9	115	96.6	17.2	40.7	32.6	136	1142	3.58	0.23	702	9.6	2.9
Es <sub>4</sub>	4186.9	5.81	7.17	20.24	0.68	1.78	0.13	7.85	105	54.3	12.8	27.4	19.2	64.4	794	3.6	0.09	624	6.9	3.3
Es <sub>4</sub>	4187.88	4.87	3.38	7.23	1.28	3.08	0.04	12.9	133	93.3	18.2	45.4	41.2	151	554	4.88	0.21	570	12.9	2.9
Es <sub>4</sub>	4188.92	4.60	3.32	8.98	1.33	2.63	0.06	11.8	137	84.1	17.5	28.6	74.6	113	660	3.91	0.16	570	12.5	3.7
Es <sub>4</sub>	4190.15	5.68	5.03	12.45	1.13	2.32	0.09	10.2	107	80.3	14.5	34.1	28	134	639	4.41	0.17	536	9.0	2.6

Fm, Formation.

of normalized erbium to neodymium (Er/Nd)<sub>N</sub> vary from 0.41 to 1.15 (average 0.85) and from 0.43 to 0.70 (mean 0.53) for Es<sub>3</sub> and Es<sub>4</sub> samples, respectively. A positive correlation can be observed between the contents of rare elements (ΣREE, LREE, and HREE) and the elements Al or Ti (Figure 5), which indicates that rare earth elements may be mainly associated with clay minerals.

## DISCUSSION

### Organic Characteristics of Source Rocks

For example, TOC and Rock-Eval S<sub>2</sub> values are commonly combined to evaluate the hydrocarbon-generating potential (Espitalié et al., 1977), and good petroleum source rocks are characterized by relatively higher TOC and S<sub>2</sub> values (Espitalié

et al., 1977; Peters, 1986). The analyzed Es samples have a TOC >0.5 wt%, which is generally accepted as the boundary between source and non-source rocks for mudstones (Jones, 1987). Hao et al. (2009b) proposed a cross plot of S<sub>2</sub> and TOC to estimate the quality of lacustrine source rocks in the BBB. It can be inferred that both the Es<sub>3</sub> and Es<sub>4</sub> samples are scattered in the range of poor to fair source rock (Figure 3), which is obviously lower than that of the Es<sub>1</sub> source rock in the Raoyang sag. The relatively lower HI values for the Es source rock in this study are consistent with previous geochemical investigations of cuttings from other drilled wells in the Langgu sag (Diao et al., 2014). This indicates low to medium petroleum potential for the source rock intervals in the Langgu sag.

## Paleoclimate

The distribution and relative concentrations of minerals and some elements in mudstones may record the changes in paleoclimate (Sheldon and Tabor, 2009; Cao et al., 2012; Goldberg and Humayun, 2010; Liu et al., 2018a; Liu et al., 2018b; Wang P. et al., 2020). Chemical weathering on continents is primarily controlled by moisture and temperature levels, and weathering intensity is generally low in arid climates (Nesbitt and Markovics, 1997; Wang Q. et al., 2020). Feldspar is mechanically less stable and is also more susceptible than quartz to chemical weathering (Kamp, 2010), so the relative variations in quartz and feldspar content in non-marine shales may reflect paleoclimatic changes (Harris, 2000; Kamp, 2010). The Es<sub>4</sub> samples seem more focused and have relatively lower Q/F values than the Es<sub>3</sub> samples (Figure 6), which may indicate changes in climate. In addition, the Es<sub>4</sub> samples show relatively high concentrations of carbonate minerals (Figure 6). Abundant carbonate deposition under an arid climate is reported in previous studies of lacustrine source rocks (e.g., Hao et al., 2011). Mineralogical compositions may indicate limited chemical weathering accompanied by an arid climate during the deposition of Es<sub>4</sub> rocks.

The Fe, Mn, Cr, V, Ni, and Co elements are believed to be enriched under moist conditions, whereas the Ca, Mg, K, Na, Sr, and Ba are mainly concentrated under arid conditions (Cao et al., 2012; Zhao et al., 2007). As a result, the ratio of  $\Sigma(\text{Fe} + \text{Mn} + \text{Cr} + \text{V} + \text{Ni} + \text{Co})/\Sigma(\text{Ca} + \text{Mg} + \text{K} + \text{Na} + \text{Sr} + \text{Ba})$  (termed as C-value) can be used to study the paleoclimate (Zhao et al., 2007), and an increase in C-values can be observed from arid climate to semimist/moist climate (e.g., Cao et al., 2012). The Es<sub>4</sub> samples displayed relatively lower C-values (0.07–0.26) than those of the Es<sub>3</sub> samples (0.17–0.44), indicating a more arid climate prevailed in the deposition of Es<sub>4</sub> source rock (Figure 6). The CIA provides a proxy for determining climate change (Cao et al., 2019; Wang P. et al., 2020). High CIA ratios generally indicate enhanced chemical weathering intensity in humid climates (Goldberg and Humayun, 2010; Cao et al., 2019; Wang P. et al., 2020). As shown in Figure 6, the relatively lower CIA values for Es<sub>4</sub> samples indicate an arid-prone climate, which is consistent with results inferred from other proxies.

The Ti-normalized ratios are commonly utilized to estimate the influence of chemical weathering (Nesbitt and Markovics,

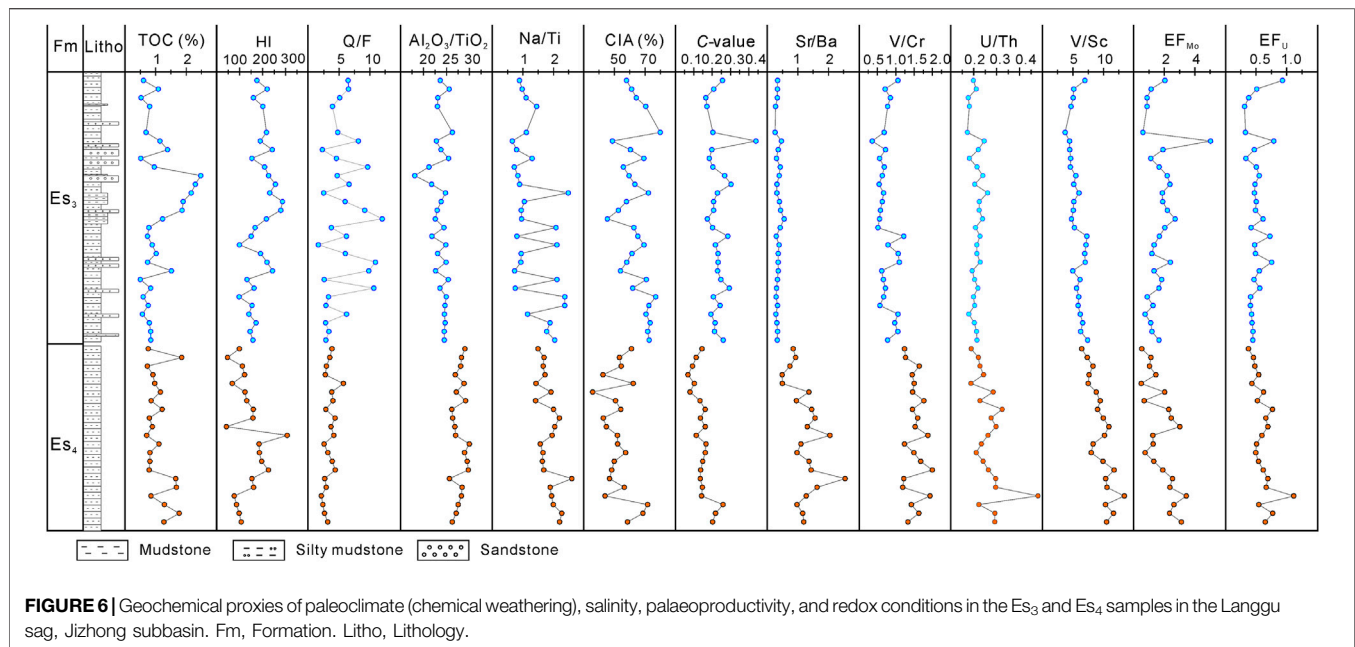
1997). The Al/Ti is proposed to document the climatic variations (Wei et al., 2004; Kiipli et al., 2012) in marine sediments, and an increase in the Al/Ti ratio can be observed in more arid climates (Akul'shina, 1976). According to Akul'shina (1976), the Al/Ti ratio <20, 20–30, and >30 represent humid, semi-humid, semi-arid, and arid climates, respectively. Similarly, the Al/Ti is also reported to reconstruct the paleoclimate/paleoenvironment of the catchment in lake settings (Haberzettl et al., 2008; Warriar and Shankar, 2009). The overall higher Al/Ti ratios for Es<sub>4</sub> samples indicate a more arid paleoclimate during the deposition period (Figure 6). In comparison, the Es<sub>3</sub> samples are deposited under humid and semi-humid paleoclimates according to this gradation. The Na/Ti ratio is another indicator of chemical weathering, and a relatively high Na/Ti ratio may reflect weak chemical weathering accompanied by a dry climate (Wei et al., 2004). The slightly higher but focused Na/Ti ratios for Es<sub>4</sub> samples further suggest an arid-prone climate.

## Paleosalinity

Salinity is an essential chemical property of lake water masses and is routinely reported in paleoenvironmental studies (Jaraula et al., 2014; Li and Liu, 2014; Wei and Algeo, 2020). Based on a large set of modern aqueous and sedimentary chemical data representing a range of salinity facies (i.e., freshwater, brackish, and marine), Wei and Algeo (2020) proposed some elemental ratios (e.g., Sr/Ba) for paleosalinity reconstruction. With increasing salinity, Ba is preferentially precipitated as a sulphate compound compared to Sr (Vosoughi Moradi et al., 2016). Moreover, Sr is present in higher concentrations in seawater and is readily adsorbed onto clay minerals, resulting in substantially higher Sr/Ba ratios in marine sediments relative to freshwater sediments (Wei and Algeo, 2020). Therefore, the Sr/Ba ratio is usually used to characterize paleosalinity, and sedimentary ratios of <0.2, 0.2–0.5, and >0.5 are indicative of freshwater, brackish, and marine facies, respectively (Wei and Algeo, 2020). As shown in Figure 8, the Es<sub>4</sub> samples generally have higher Sr/Ba values than the Es<sub>3</sub> samples, suggesting high paleosalinity during Es<sub>4</sub>'s deposition, which is consistent with the arid climate. Gammacerane/C<sub>30</sub>hopane (G/H) is commonly utilized to evaluate water-column stratification during the deposition of source rocks (Sinninghe et al., 1995). Although both hypersalinity at depth and temperature gradients may result in a stratified water column (Bohacs et al., 2000), high G/H ratios are mostly found in evaporite or other high salinity in lacustrine depositional environments (Fu et al., 1990; Chen et al., 1996; Hao et al., 2011). According to Diao et al. (2014), the Es<sub>4</sub> source rock has obviously higher G/H ratios (0.4–0.41) than that of the Es<sub>3</sub> source rock (0.04–0.26) in the Langgu sag. This agrees well with the interpretation of paleosalinity based on elements, indicating high paleosalinity and relatively high preservation favored by water-column stratification.

## Hydrological Conditions

Previous research suggested that the Er/Nd ratios display a positive correlation with PH of seawater (Goldstein and Jacobsen, 1987). In this study, the Es<sub>3</sub> samples have obviously higher (Er/Nd)<sub>N</sub> values than those in Es<sub>4</sub> (Figure 5), which seems



to be inconsistent with acidic and freshwater to brackish water during Es<sub>3</sub>'s deposition (e.g., Diao et al., 2014). This indicates that caution should be exercised when applying this ratio to estimate the PH of lake waters because this variable trend is generally complicated by water types associated with hydrological conditions (Elderfield et al., 1990). Nevertheless, given the differences in paleoclimate and paleosalinity between Es<sub>4</sub> and Es<sub>3</sub> samples, the (Er/Nd)<sub>N</sub> may provide a potential proxy to characterize changes in the hydrological conditions.

The  $\delta^{13}\text{C}_{\text{Carb}}$  and  $\delta^{18}\text{O}_{\text{Carb}}$  values of primary carbonates are proved a useful technique for paleolimnological research (Talbot, 1990; Pérez et al., 2013). The systematic decrease in  $\delta^{13}\text{C}_{\text{Carb}}$  for Es<sub>3</sub> samples suggests the input of isotopically depleted carbon derived from soil CO<sub>2</sub> and in turn from the decay of vegetation (Harris et al., 2004), which is consistent with a more humid paleoclimate during the Es<sub>3</sub>'s deposition. The oxygen isotope values in lacustrine carbonates are commonly influenced by the temperature and the  $\delta^{18}\text{O}$  value of the lake water (Talbot, 1990; Dettman et al., 2003; Pérez et al., 2013), with the latter controlled by hydrological conditions. Based on studies of modern and ancient lakes, Talbot (1990) proposed that carbonates show little or no correlation between  $\delta^{13}\text{C}_{\text{Carb}}$  and  $\delta^{18}\text{O}_{\text{Carb}}$  in a hydrologically open lake, whereas carbonates from a hydrologically closed lake may display covarying  $\delta^{13}\text{C}_{\text{Carb}}$  and  $\delta^{18}\text{O}_{\text{Carb}}$ , although differences in covariant trend may exist among different lakes (Talbot, 1990). Other studies of ancient and modern lakes also confirmed isotopic covariances in hydrologically closed conditions (Fontes et al., 1996; Sinha et al., 2006; Yin et al., 2018). As shown in **Figure 9**, the  $\delta^{13}\text{C}_{\text{Carb}}$  and  $\delta^{18}\text{O}_{\text{Carb}}$  exhibit an approximate positive correlation. In comparison, the Es<sub>3</sub> samples have very little variation in  $\delta^{13}\text{C}_{\text{Carb}}$  and  $\delta^{18}\text{O}_{\text{Carb}}$ , with no isotopic covariance (**Figure 9**). This indicates that the Es<sub>4</sub> source rocks were deposited under relatively hydrologically closed conditions when compared

to the Es<sub>3</sub> rocks. Although the  $\delta^{13}\text{C}_{\text{Carb}}$  values may also be influenced by other factors (e.g., climate and biological processes) (Hollander and McKenzie, 1991; Hollander et al., 1992), covariant trends can be generally utilized to trace the hydrological history of a basin with caution. That the relatively closed hydrological conditions during the Es<sub>4</sub>'s deposition are also consistent with the geological setting and other geochemical proxies discussed above.

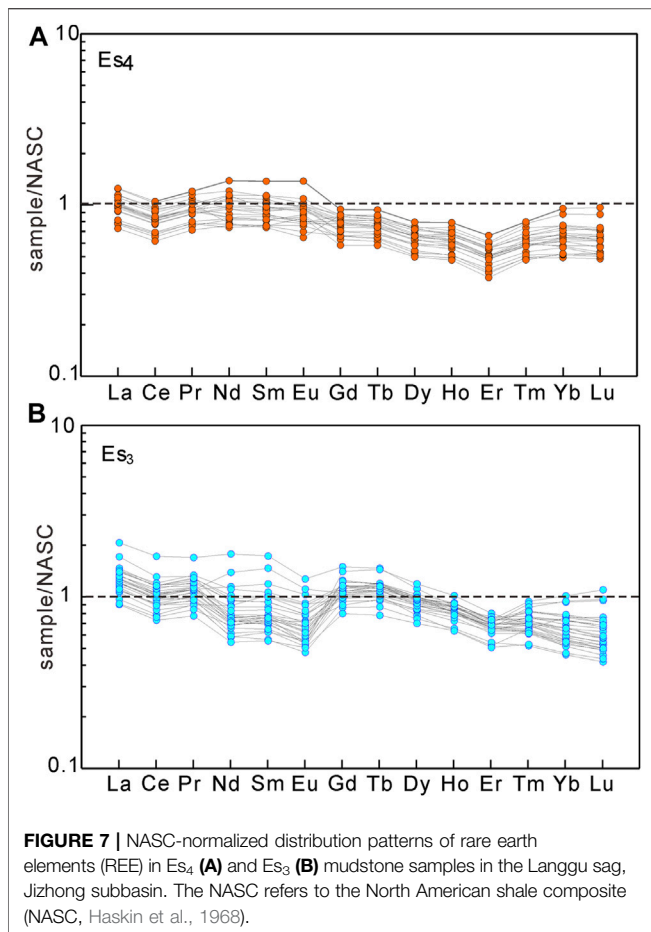
## Productivity and Redox Conditions

As discussed above, the paleoclimate during the deposition of Es<sub>3</sub> is humid-prone, and enhanced water inflow may have efficiently carried nutrients to the lake, which is favorable for algal blooms. During photosynthesis, <sup>12</sup>C is preferentially incorporated into organic matter; however, the dissolved inorganic carbon source may be used due to limited concentrations of dissolved carbon dioxide (e.g., Hollander and McKenzie, 1991). Thus, high productivity may reduce isotopic fractionation between dissolved inorganic carbon and particulate organic carbon. As shown in **Figure 5**, the Es<sub>3</sub> samples display heavier  $\delta^{13}\text{C}_{\text{OM}}$  than those of Es<sub>4</sub>. The <sup>13</sup>C-enriched  $\delta^{13}\text{C}_{\text{OM}}$  associated with high productivity has also been reported in previous studies of lacustrine deposits (e.g., Yin et al., 2018) (Hollander and McKenzie, 1991; Wang Q. et al., 2020). The carbon isotope of organic matter in the Shahejie Formation in Bozhong Sag is obviously the heaviest, followed by the third member of the Shahejie Formation in Langgu Sag, and the fourth member of the Shahejie Formation in Langgu Sag and the first member of the Shahejie Formation in Raoyang Sag are the lightest (**Figure 10**). It is generally accepted that the heavy organic carbon isotope of source rock in the Shahejie Formation in Bozhong Sag is mainly caused by high primary productivity (e.g., Yin et al., 2020). Similarly, the heavy carbon isotope of source rocks in Es<sub>3</sub> in Langgu Sag can also reflect high paleoproductivity. Therefore, the

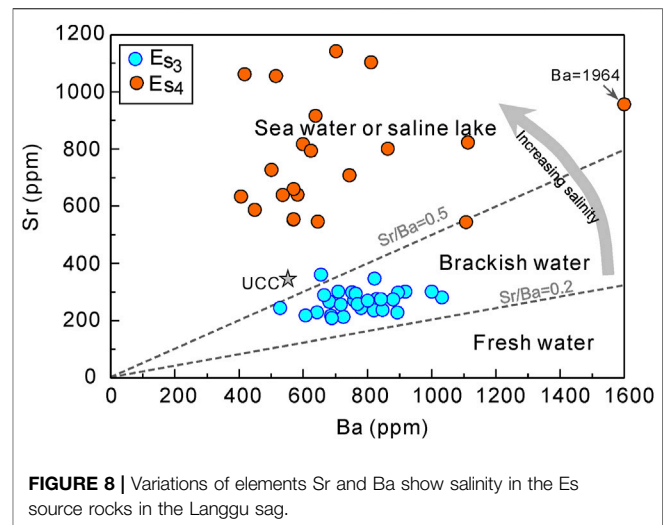
**TABLE 3 |** Rare earth element concentrations ( $\mu\text{g/g}$ ) and corresponding calculated parameters of  $\text{Es}_3$  and  $\text{Es}_4$  mudstone in the Langgu sag.

Fm	Depth (m)	La	Ce	Pr	Nd	Sm	Eu	Gd	Tb	Dy	Ho	Er	Tm	Yb	Lu	$\Sigma\text{REE}$	HREE	LREE	L/H	$(\text{La/Yb})_N$	$(\text{Er/Nd})_N$
$\text{Es}_3$	3407.5	66.3	126	13.4	58.8	9.87	1.58	7.80	1.25	5.58	0.92	2.50	0.47	3.15	0.53	298	22.2	276.0	12.4	2.04	0.41
$\text{Es}_3$	3408.75	42.7	79.1	9.02	25.2	4.46	0.78	6.35	1.02	5.00	0.90	2.37	0.35	1.86	0.26	179	18.1	161.3	8.9	2.22	0.91
$\text{Es}_3$	3410.7	45.9	83.6	9.14	24	3.94	0.69	6.5	1.01	4.84	0.85	2.26	0.31	1.64	0.24	185	17.7	167.3	9.5	2.71	0.91
$\text{Es}_3$	3411.6	47.1	85.7	9.46	24.3	4.1	0.72	6.42	1.01	5.02	0.84	2.25	0.31	1.6	0.22	189	17.7	171.4	9.7	2.85	0.90
$\text{Es}_3$	3553.3	54.9	95.7	10.4	25.8	4.29	0.67	7.32	1.23	5.96	1.06	2.73	0.35	1.72	0.25	212	20.6	191.8	9.3	3.09	1.03
$\text{Es}_3$	3556.8	31	57.6	7.14	29.4	5.84	1.12	5.08	0.86	3.91	0.67	1.77	0.33	2.36	0.37	147	15.3	132.1	8.6	1.27	0.58
$\text{Es}_3$	3563.38	39	71.4	7.68	20.3	3.61	0.64	5.59	0.98	4.73	0.85	2.25	0.31	1.6	0.22	159	16.5	142.6	8.6	2.36	1.08
$\text{Es}_3$	3565.5	43.1	76.4	8.74	23	4.02	0.66	6.01	0.99	4.9	0.87	2.32	0.32	1.76	0.24	173	17.4	155.9	9.0	2.37	0.98
$\text{Es}_3$	3567.8	36.3	65.7	7.18	19.3	3.56	0.69	5.6	0.97	4.73	0.85	2.29	0.32	1.67	0.24	149	16.7	132.7	8.0	2.11	1.15
$\text{Es}_3$	3571.2	38.6	71	8.4	23.7	4.17	0.84	6.01	0.99	5.03	0.90	2.4	0.34	1.8	0.25	164	17.7	146.7	8.3	2.08	0.98
$\text{Es}_3$	3571.7	37.4	69.8	7.88	22.8	4.08	0.74	5.78	1.02	5.18	0.96	2.51	0.37	1.96	0.28	161	18.0	142.7	7.9	1.85	1.07
$\text{Es}_3$	3571.95	40.7	74.5	8.94	25.2	4.23	0.79	5.39	0.89	4.58	0.85	2.21	0.34	1.83	0.26	171	16.3	154.4	9.4	2.15	0.85
$\text{Es}_3$	3572.4	35	66.5	7.49	21.8	3.7	0.67	4.91	0.81	4.15	0.76	2.16	0.32	1.72	0.24	150	15.1	135.2	9.0	1.97	0.96
$\text{Es}_3$	3572.8	34	61.3	7.06	19.5	3.22	0.59	4.51	0.74	3.74	0.68	1.85	0.26	1.43	0.20	139	13.4	125.7	9.4	2.30	0.92
$\text{Es}_3$	3573.35	28.9	53.5	6.13	18	3.17	0.63	4.16	0.67	3.51	0.66	1.73	0.27	1.46	0.21	123	12.7	110.3	8.7	1.92	0.93
$\text{Es}_3$	3573.85	38.6	73	8.73	26.1	4.48	0.90	5.36	0.84	4.21	0.79	2.09	0.31	1.7	0.24	167	15.5	151.8	9.8	2.20	0.78
$\text{Es}_3$	3574.7	40.9	74.1	8.73	37.9	6.79	1.28	5.23	0.86	4.45	0.87	2.39	0.46	2.89	0.46	187	17.6	169.7	9.6	1.37	0.61
$\text{Es}_3$	3575.6	29.2	55.8	6.67	22.5	4.2	0.89	4.66	0.82	4.25	0.83	2.33	0.38	2.14	0.32	135	15.7	119.3	7.6	1.32	1.01
$\text{Es}_3$	3577.43	38.4	71.5	8.35	24.9	4.47	0.84	5.99	0.97	4.96	0.92	2.36	0.36	1.95	0.28	166	17.8	148.5	8.3	1.91	0.92
$\text{Es}_3$	3577.9	40.4	76.5	8.68	45.9	8.39	1.38	5.48	0.93	4.47	0.87	2.26	0.44	2.93	0.47	199	17.8	181.3	10.2	1.34	0.48
$\text{Es}_3$	3578.93	34.7	67	7.93	24	4.35	0.83	5.16	0.87	4.46	0.83	2.18	0.36	2.05	0.28	155	16.2	138.8	8.6	1.64	0.88
$\text{Es}_3$	3580.1	45	84.7	9.8	31.3	5.34	0.98	5.94	0.96	4.82	0.90	2.61	0.38	2.27	0.33	195	18.2	177.1	9.7	1.92	0.81
$\text{Es}_3$	3620.1	39.7	75.5	8.79	28.9	4.98	0.97	5.64	0.93	4.88	0.95	2.52	0.42	2.36	0.34	177	18.0	158.8	8.8	1.63	0.85
$\text{Es}_3$	3621.14	35.6	65.1	7.57	23.5	4.31	0.77	5.36	0.92	4.69	0.92	2.37	0.36	2.04	0.30	154	17.0	136.8	8.1	1.69	0.98
$\text{Es}_3$	3621.89	41.1	76.7	8.96	27.4	4.8	0.87	5.52	0.93	4.45	0.82	2.35	0.35	2.04	0.29	177	16.7	159.8	9.5	1.95	0.83
$\text{Es}_3$	3622.7	42.3	81.7	9.6	31.5	5.33	0.98	5.47	0.92	4.6	0.91	2.45	0.41	2.42	0.34	189	17.5	171.4	9.8	1.69	0.75
$\text{Es}_3$	3624.73	45.7	87.9	10.6	36.6	6.08	1.14	6.03	0.99	4.79	0.96	2.47	0.41	2.45	0.35	206	18.5	188.0	10.2	1.81	0.66
$\text{Es}_3$	3625.7	44.8	84.6	10.1	33.7	5.69	1.11	5.88	0.95	4.83	0.91	2.34	0.38	2.27	0.32	198	17.9	180.0	10.1	1.91	0.67
$\text{Es}_3$	3627.4	44.8	84.9	10.2	32.2	5.7	1.03	6.05	0.98	4.94	0.95	2.51	0.38	2.25	0.33	197	18.4	178.8	9.7	1.93	0.76
$\text{Es}_4$	4119.4	36.5	69.2	8.07	25.7	4.21	0.80	4.55	0.73	3.67	0.69	1.86	0.30	1.78	0.26	158	13.8	144.5	10.4	1.99	0.70
$\text{Es}_4$	4120.3	31.5	59	7.32	36.4	6.14	1.19	4.22	0.69	3.41	0.65	1.74	0.29	2.01	0.31	155	13.3	141.6	10.6	1.52	0.46
$\text{Es}_4$	4121.3	32	61.6	7.38	27.9	4.87	0.98	4.2	0.66	3.24	0.65	1.7	0.30	1.79	0.28	148	12.8	134.7	10.5	1.73	0.59
$\text{Es}_4$	4122.6	25.2	50.2	6.13	24.4	4.3	0.87	3.44	0.57	2.93	0.58	1.54	0.27	1.75	0.25	122	11.3	111.1	9.8	1.40	0.61
$\text{Es}_4$	4124	36.6	70.6	8.57	31.3	5.04	0.98	4.48	0.69	3.56	0.71	1.92	0.32	2.08	0.30	167	14.1	153.1	10.9	1.70	0.60
$\text{Es}_4$	4124.62	25.1	49.1	6.2	25.4	4.34	0.94	3.42	0.54	2.63	0.53	1.39	0.25	1.53	0.23	122	10.5	111.1	10.6	1.59	0.53
$\text{Es}_4$	4125.32	31.7	62	7.5	29.2	4.97	1.01	3.84	0.62	3.12	0.63	1.69	0.31	2	0.31	149	12.5	136.4	10.9	1.54	0.56
$\text{Es}_4$	4125.72	34.1	66.1	8.07	35.1	5.91	1.22	4.29	0.69	3.33	0.71	1.89	0.33	2.29	0.34	164	13.9	150.5	10.9	1.44	0.52
$\text{Es}_4$	4127.42	24.7	47.6	5.97	27.1	4.62	1.09	3.27	0.52	2.53	0.51	1.36	0.25	1.59	0.24	121	10.3	111.1	10.8	1.50	0.49
$\text{Es}_4$	4128.42	26.1	50.7	6.32	27.4	4.68	1.05	3.43	0.55	2.71	0.53	1.45	0.26	1.6	0.25	127	10.8	116.3	10.8	1.58	0.51
$\text{Es}_4$	4130.44	31.7	60.8	7.54	37.4	5.44	1.21	3.98	0.63	3.15	0.61	1.65	0.29	1.97	0.30	157	12.6	144.1	11.5	1.56	0.43
$\text{Es}_4$	4132.59	30.8	58.7	7.25	27.8	4.68	0.97	4.03	0.65	3.31	0.64	1.67	0.30	1.91	0.27	143	12.8	130.2	10.2	1.56	0.58
$\text{Es}_4$	4133.44	35.4	67.8	8.22	34.8	5.81	1.22	4.58	0.73	3.74	0.74	2.03	0.37	2.35	0.34	168	14.9	153.3	10.3	1.46	0.57
$\text{Es}_4$	4134.8	31.4	60.2	7.44	32.7	5.56	1.16	4.13	0.64	3.3	0.65	1.72	0.31	2.08	0.32	152	13.2	138.5	10.5	1.46	0.51
$\text{Es}_4$	4135.84	29.4	56.3	6.98	32.3	5.34	1.17	3.64	0.58	2.98	0.60	1.7	0.31	2.12	0.32	144	12.2	131.5	10.7	1.34	0.51
$\text{Es}_4$	4184.25	29.6	56.9	7.01	31.3	5.24	1.19	3.67	0.60	2.91	0.61	1.64	0.29	1.91	0.30	143	11.9	131.2	11.0	1.50	0.51
$\text{Es}_4$	4185.8	32.6	60.8	7.43	32.7	5.56	1.13	4.09	0.63	3.3	0.68	1.89	0.33	2.21	0.35	154	13.5	140.2	10.4	1.43	0.56
$\text{Es}_4$	4186.9	23.4	45	5.65	25.1	4.3	1.04	3.03	0.49	2.49	0.50	1.28	0.24	1.61	0.25	114	9.9	104.5	10.6	1.41	0.49
$\text{Es}_4$	4187.88	39.8	74.8	9.07	39.9	6.39	1.27	4.44	0.70	3.67	0.77	2.07	0.39	2.74	0.42	186	15.2	171.2	11.3	1.41	0.50
$\text{Es}_4$	4188.92	40	76.6	9.5	45.8	7.85	1.71	4.9	0.80	3.97	0.82	2.26	0.40	2.96	0.46	198	16.6	181.5	11.0	1.31	0.48
$\text{Es}_4$	4190.15	32.7	62.4	8.03	37.7	6.47	1.35	4.54	0.74	3.61	0.72	1.93	0.35	2.36	0.35	163	14.6	148.7	10.2	1.34	0.50

Fm, Formation;  $\Sigma\text{REE}$ , Total concentrations of rare earth elements; LREE, refers to total content of light rare earth elements ( $\text{LREE} = \text{La} + \text{Ce} + \text{Pr} + \text{Nd} + \text{Sm} + \text{Eu}$ ); total HREE, refers to content of heavy rare earth elements ( $\text{HREE} = \text{Gd} + \text{Tb} + \text{Dy} + \text{Ho} + \text{Er} + \text{Tm} + \text{Yb} + \text{Lu}$ ); L/H = LREE/HREE. N refers to ratios of normalized concentrations against the North American Shale Composite (NASC, Haskin et al., 1968).



overall enrichment in  $\delta^{13}\text{C}_{\text{OM}}$  in the Es<sub>3</sub> samples may indicate high primary productivity under a relatively humid climate. Although Ba is commonly used to characterize primary production in seawater (Dymond et al., 1992), the Ba-bio provides an indicator of primary productivity in lacustrine settings (Wang Q. et al., 2020; Yin et al., 2020). High productivity is commonly accompanied by higher Ba-bio values (e.g., Neuhuber et al., 2016; Yin et al., 2020). Despite the wide range of Ba-bio values of Es<sub>4</sub> samples, the Es<sub>3</sub> samples display relatively higher Ba-bio values (Figure 5), which is consistent with higher primary productivity. Nevertheless, the Ba-bio values of Es in this study are more than two times lower than those of the Es<sub>3</sub> rock in the Bozhong region, where productivity was dominant (Yin et al., 2020). This indicates that the primary productivity may be limited in the Langgu, although there exists a general difference in productivity between Es<sub>3</sub> and Es<sub>4</sub> samples. Biogenic silica concentration is also a useful proxy of paleoproductivity, and higher primary productivity is commonly accompanied by enhanced Si-bio values (e.g., Ross and Bustin, 2009). The overall higher values of Si-bio for Es<sub>3</sub> samples may suggest increased productivity (Figure 5). Note that these suggested useful proxies of paleoproductivity of marine background display rather complex vary trends for lacustrine sediments (Figure 5), similar phenomena were also reported in



other studies (e.g., Cao et al., 2012). This indicates that the element compositions have complex controlling factors other than paleoproductivity, thus caution should be exercised when evaluating productivity for lacustrine sequences.

According to the study (Katz, 2001), high-quality source rock seems to be more associated with good preservation conditions at a prerequisite of productivity. Cr is commonly incorporated within detrital sediments, whereas V is usually concentrated in organic-rich sediments that are deposited under reducing conditions (Shaw et al., 1990; Makeen et al., 2015). Thus, V/Cr is a proxy used to compare the redox conditions (Jones and Manning, 1994), and V/Cr ratios higher than 2.0 may be an indicator of anoxic depositional conditions (Makeen et al., 2015). Additionally, the U/Th ratio is commonly suggested to interpret paleo-oxygenation conditions, with dysoxic and anoxic conditions showing U/Th ratios higher than 0.75 and 1.25, respectively (Jones and Manning, 1994). As displayed in Figure 6, the Es<sub>4</sub> and Es<sub>3</sub> samples have V/Cr and U/Th not exceeding 2.0 and 0.75, respectively, suggesting a less reducing environment during deposition. However, the Es<sub>4</sub> samples exhibit relatively higher V/Cr and U/Th values than those of the Es<sub>3</sub> samples (Figure 6), which indicate relatively enhanced reducing environments during Es<sub>4</sub>'s deposition. In comparison, the V/Sc seems to be a more sensitive and reliable proxy for paleoredox conditions (Kimura and Watanabe, 2001; Wang Q. et al., 2020). V/Sc values  $\geq 9.1$  may indicate a low-oxygen depositional environment (Kimura and Watanabe, 2001; Powell, 2009). Compared to the Es<sub>3</sub> samples, the Es<sub>4</sub> samples display obviously higher V/Sc values (Figure 6 and Table 1), suggesting promoted anoxic conditions during the deposition of Es<sub>4</sub>, which is consistent with the relatively low values of Pr/Ph for the Es<sub>4</sub> source rock (Diao et al., 2014).

The relative abundance of the redox-sensitive elements molybdenum (Mo) and uranium (U) are commonly used to characterize the marine sediment depositions (e.g., Algeo and Tribouillard, 2009), whereas many studies showed that Mo and U are also applicable to the research of lake sedimentary environments (Harris et al., 2004; Dahl et al., 2013; Yin et al.,

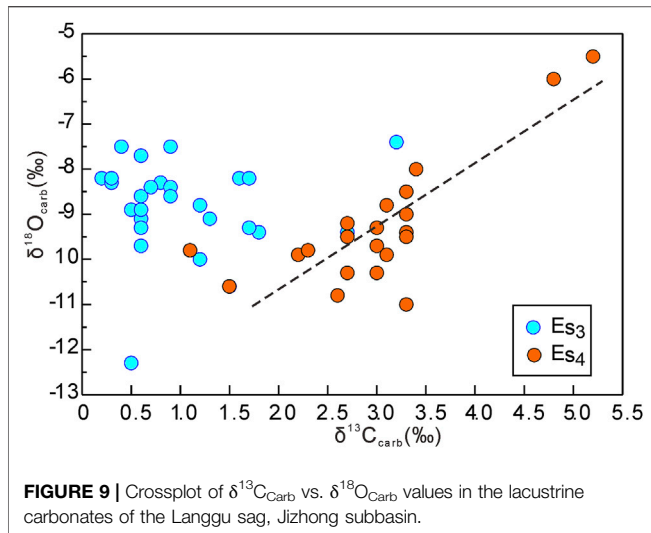


**FIGURE 9** | Crossplot of  $\delta^{13}\text{C}_{\text{carb}}$  vs.  $\delta^{18}\text{O}_{\text{carb}}$  values in the lacustrine carbonates of the Langgu sag, Jizhong subbasin.

2018). Although the  $\text{Es}_4$  and  $\text{Es}_3$  samples display a similar range of  $\text{EF}_{\text{Mo}}$  and  $\text{EF}_{\text{U}}$  values, the  $\text{Es}_4$  samples are characterized by a slight enrichment of Mo and U, which may indicate relatively oxygen-deficient conditions. The complex variations in redox-sensitive proxies of the Es samples may imply variable redox conditions in the Langgu area. Previous studies have confirmed that the  $\text{EF}_{\text{Mo}}$  and  $\text{EF}_{\text{U}}$  values in lake settings may be influenced by the variability of the detrital input (e.g., Yin et al., 2018). Compared to the  $\text{Es}_1$  source rocks (Raoyang sag) deposited under anoxic bottom water conditions with stable water-column stratification, the  $\text{Es}_4$  and  $\text{Es}_3$  samples in the Langgu sag display obviously lower  $\text{EF}_{\text{Mo}}$  and  $\text{EF}_{\text{U}}$  ratios (Figure 11). It is assumed that the analyzed Es source rocks are deposited under a less anoxic bottom with a significant influence of detrital input (see below Discussion). Nevertheless, combined with other redox proxies, it can be generally concluded that the  $\text{Es}_4$  rocks are deposited under relatively reducing environments, which may provide relatively good preservation conditions for organic matter.

## Mechanisms of Source Rock Occurrence

Based on the statistics between HI and carbon isotopic fractionation between carbonate and kerogen ( $\Delta\delta^{13}\text{C}_{\text{carb-OM}}$ ), Hollander et al. (1993) proposed an idealized cross-plot to identify two controlling factors (productivity and preservation) of the accumulation of organic carbon-rich matter. A negative and positive trend between  $\Delta\delta^{13}\text{C}_{\text{carb-OM}}$  and HI was observed when the controlling factors in the enrichment of organic matter were high productivity and enhanced preservation, respectively. These two varying trends were also observed in rift sequences in other sedimentary basins (Gonçalves, 2002; Liu et al., 2017; Yin et al., 2018; Wang Q. et al., 2020). Figure 12 shows that the  $\text{Es}_4$  samples present a positive trend of  $\Delta\delta^{13}\text{C}_{\text{carb-OM}}$  with HI values, suggesting that increased preservation (relatively stable stratified water conditions) may have been responsible for the formation of the potential source rock. This is consistent with higher paleosalinity and enhanced reducing conditions. In comparison, the  $\Delta\delta^{13}\text{C}_{\text{carb-OM}}$  and HI values of the  $\text{Es}_3$

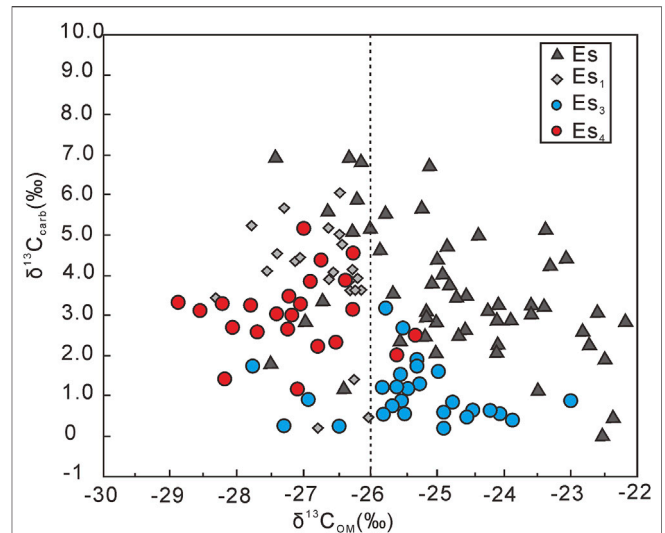
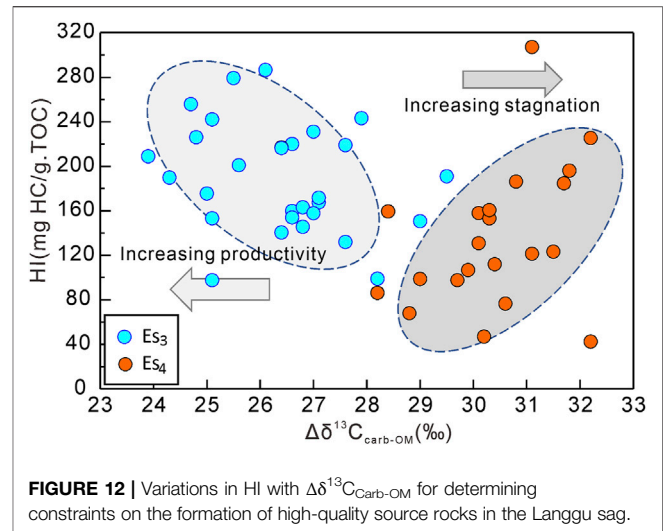
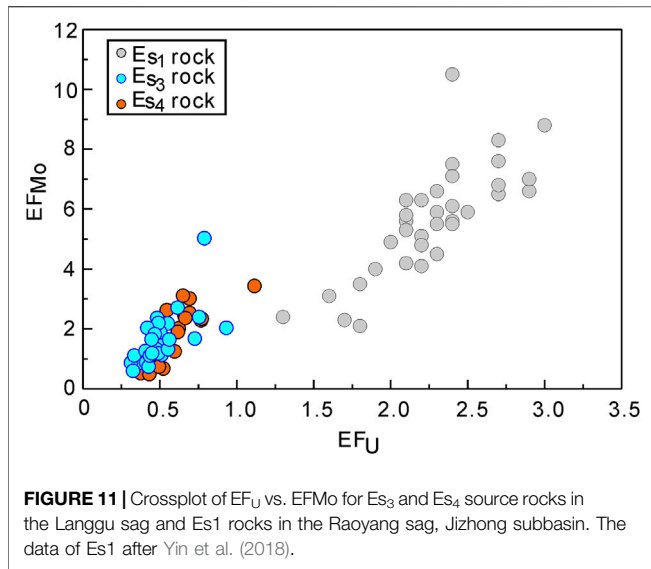


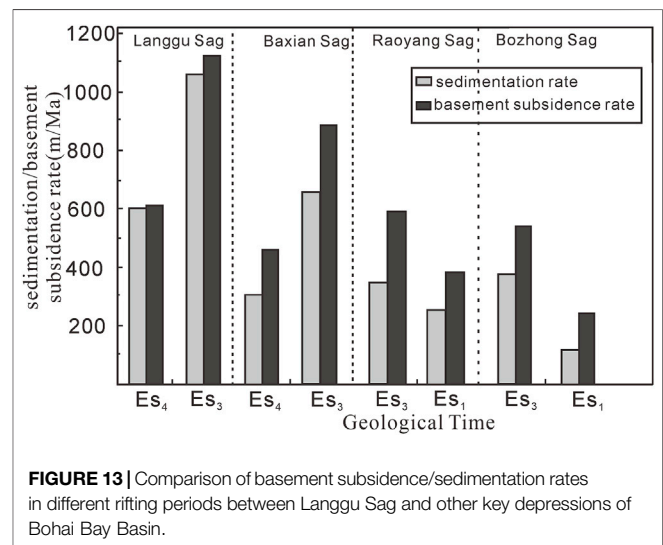
**FIGURE 10** | Crossplot  $\delta^{13}\text{C}_{\text{om}}$  values of vs.  $\delta^{13}\text{C}_{\text{carb}}$  values for  $\text{Es}_3$  and  $\text{Es}_4$  rock samples from the Langgu sag, Jizhong subbasin. The Es source rock samples from the Bozhong sag (Yin et al., 2020) and the  $\text{Es}_1$  source rock samples from the Raoyang sag (Yin et al., 2018) were plotted for comparison of the shift of the  $\delta^{13}\text{C}_{\text{om}}$  values to evaluate the paleoproductivity in the  $\text{Es}_3$  and  $\text{Es}_4$  rock samples.

samples generally exhibited a negative correlation, which highlights high productivity in the accumulation of organic matter. However, compared with high-quality source rock intervals in the Jizhong subbasin, the Es source rocks in the Langgu sag show limited petroleum potential (Figure 3). This implies that the effects of other geological processes on the quality of source rock should be considered apart from high productivity and enhanced preservation.

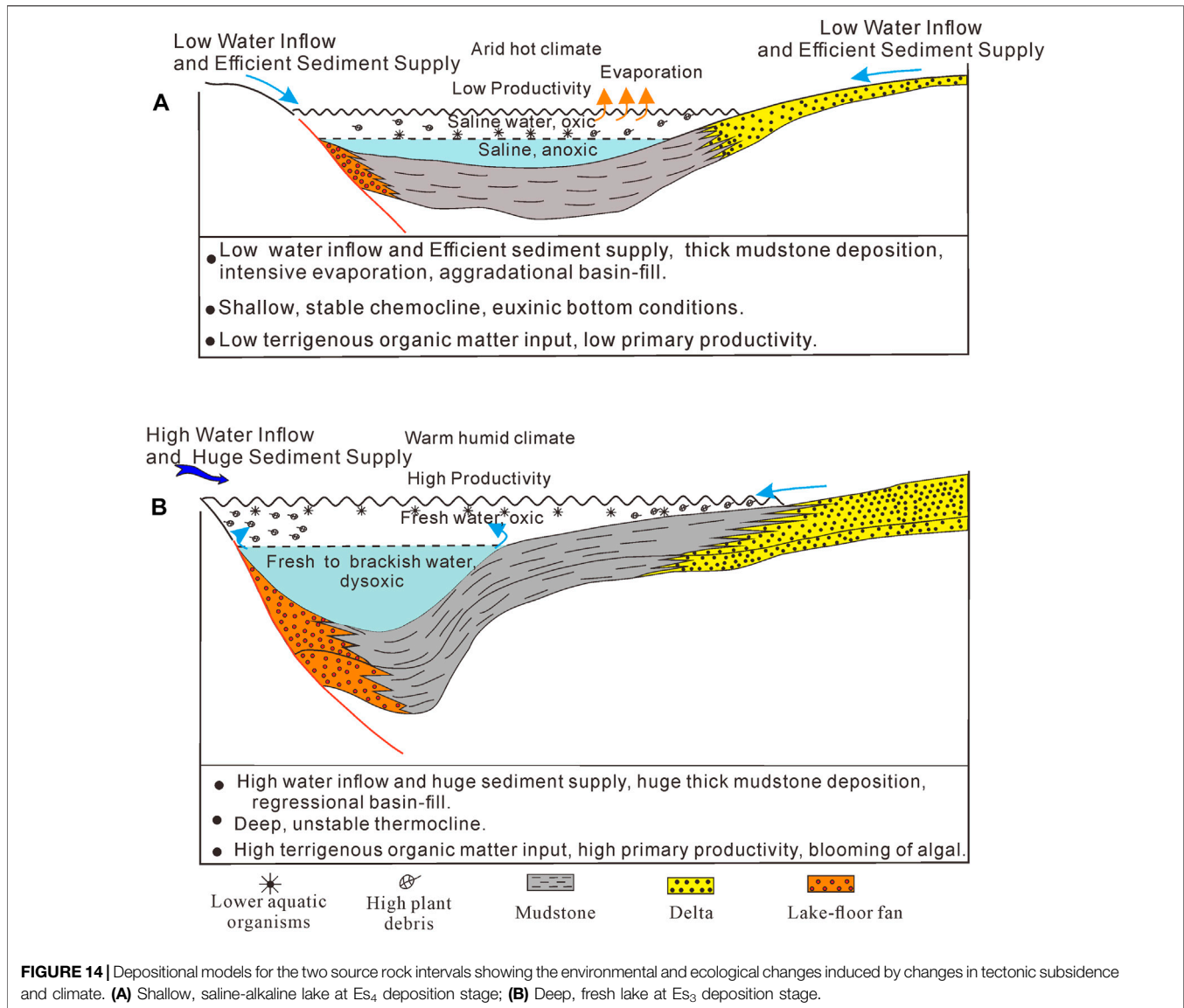
The Es source rocks in other hydrocarbon-generation rich sags (e.g., Bozhong sag, Raoyang sag, and Baxian sag) in the Bohai Bay Basin have good to excellent quality with the TOC content ranging from 2.0 to 4.0 wt% and dominant type  $\text{II}_1$  organic matter. In comparison, the Es source rock in the Langgu sag has a TOC content mainly ranging from 1.0 to 2.0 wt% and its organic matter type is mainly  $\text{II}_2\text{-III}$ , indicating low to medium petroleum potential. It is generally believed that slow deposition rates can maximize exposure time and reduce the preservation of organic matter, resulting in low organic matter content. Moreover, the remnant organic matter is mainly composed of terrigenous components, which have relatively low hydrocarbon generation potential (Tyson, 2001). The high deposition rate or burial rate reduces the exposure time of organic matter in the diagenetic zone, which promotes the preservation of oil-pouring components and enhances the hydrocarbon generation potential of source rock. However, overhigh sedimentation rates often lead to the dilution of organic matter. In fact, the accumulation of high-quality source rock is controlled by complex, non-linear interactions of primary productivity, dilution, and preservation (Bohacs et al., 2000; Bohacs et al., 2005). Previous studies pertaining to the relationships between sedimentation rates and TOC revealed that the increase in TOC content is



accompanied by enhanced sedimentation rates at slow sedimentation rates due to greater preservation resulting from more rapid burial, whereas above a critical sedimentation rate the TOC content decreases with increasing sedimentation rate, due to dilution by mineral matter (Ibach, 1982; Bustin and Chonchawalit, 1997). This indicates the non-linear relationship between TOC and sedimentation rate. Although a relatively high sedimentation rate may be beneficial for organic burial and result in enhanced TOC and HI, the abundance of organic carbon may decrease with a substantial sedimentation rate (Tyson, 2001). The sedimentation rate can be approximately estimated by the thickness of the sedimentary formation divided by the age difference between the lower and upper boundaries of the selected formation (Ibach, 1982; Zakir Hossain et al., 2009). For the tectonic evolution in the Langgu sag, the  $Es_4$  and  $Es_3$  showed strong rifting activity. The Langgu sag, which experienced multiple rifting events, displays an obviously different syn-rift basement subsidence rate and sedimentation rate than other sags in the BBB. The calculated basement subsidence rate is up to 610 m/Ma during the deposition of the  $Es_4$ , and increased to up to 1,120 m/Ma during the  $Es_3$ 's deposition (Figure 13). In comparison, the  $Es_4$  and  $Es_3$  in Langgu Sag are characterized by the maximum subsidence and deposition rates in the whole Bohai Bay Basin (Figure 13). Such high sedimentation rates not only led to the development of extremely thick lacustrine deposits but also diluted the enrichment of organic matter, resulting in the formation of source rocks with low to medium organic matter content and petroleum potential. Well 8 drilled the upper member of the  $Es_4$  to a thickness of 297 m. Based on the stratigraphic age in Figure 2, the estimated sedimentation rate (no compaction correction) for  $Es_4$  strata is 11.0 cm/1,000 years. This value may underestimate the sedimentation rate during  $Es_4$ 's deposition because the  $Es_4$  strata were not fully drilled by the well 8. According to the nearby well 5 (Figure 1B) drilled with the complete  $Es_4$  sequence, the calculated sedimentation rate of  $Es_4$  is as high as 33.9 cm/1,000 years. The well 1 drilled the complete



$Es_3$  strata with a thickness of 2,570 m and yielded an average sedimentation rate of 47.9 cm/1,000 years, which is generally higher than that of  $Es_4$ . The higher sedimentation rate for  $Es_3$  strata is also supported by the humid paleoclimate and the intense activity of the boundary fault. In addition, a higher  $(La/Yb)_N$  ratio was observed to be associated with enhanced sedimentary rates in lacustrine sediments (e.g., Li et al., 2017). The overall higher  $(La/Yb)_N$  values for the  $Es_3$  sequence (Figure 5) may also suggest a higher sedimentation rate during its deposition. In comparison, the  $Es_1$  source rock in the Raoyang sag, deposited under saline and anoxic bottom water conditions with stable water-column stratification, displays an obviously low sedimentation rate, with an estimated value of 8.8 cm/1,000 years (Yin et al., 2018). Abnormally high sedimentation rates for the  $Es$  strata ( $Es_4$  and  $Es_3$ ) in the Langgu sag indicate that the accumulation of organic matter is likely to be diluted by detrital mineral matter. This interpretation is also supported by differences in bulk mineral and element compositions between  $Es$  samples in the



Langgu (much more felsic minerals) and Es<sub>1</sub> source rock in the Raoyang sag (Figure 4). This study underscores that both high productivity and enhanced preservation are prerequisites; however, the influence of dilution plays an important role in the occurrence of high-quality source rock during the rifting stage. Source rocks with high petroleum potential may agree well with moderate sedimentation rates (Katz, 2005).

### Models for Source Rock Deposition Under Different Tectonic and Climatic Conditions

Stratigraphic and subsidence studies show that the Langgu sag experienced quick subsidence during Es<sub>4</sub> deposition (close to 610 m/Ma) and a rapid subsidence rate during Es<sub>3</sub> (up to 1,120 m/Ma) (Figure 13). The paleoclimate also changed from an arid climate during Es<sub>4</sub> deposition to a humid climate during Es<sub>3</sub> deposition. It is evident that changes in water chemistry

indicated by inorganic geochemical parameters are consistent with changes in subsidence rate and climate. More importantly, both parameters reflecting chemical conditions of ancient water bodies and parameters reflecting primary productivity covary with parameters reflecting depositional conditions, which strongly imply the coevolution of ecological systems with environments. These observed environmental and ecological changes reflected by carbon isotopes of organic matter ( $\delta^{13}\text{C}_{\text{OM}}$ ), carbon ( $\delta^{13}\text{C}_{\text{Carb}}$ ) and oxygen ( $\delta^{18}\text{O}_{\text{Carb}}$ ) isotopes of carbonate, bulk mineral compositions, and major and trace element concentrations enable us to construct models for the deposition of low to medium quality lacustrine source rocks under different tectonic and climatic conditions.

During Es<sub>4</sub> deposition, the weak activity of the border fault and low subsidence rate, together with the low water inflow and intensive evaporation in an arid climate, led to the formation of a saline, alkaline, shallower lake. Low sediment input resulted in regressional or aggradational basin-fill (Figure 14A). The strong

evaporation effect led to an increase in water salinity, which favored the establishment of stable water column stratification. Stable stratification of water can form an anoxic environment, which is extremely beneficial to the preservation of organic matter (Figure 14A). The stable water column stratification and the euxinic bottom water conditions can be evidenced from the fact that Es<sub>4</sub> has the higher Sr/Ba, V/Cr, and V/Sc in the Langgu sag. Weak chemical weathering accompanied by a dry climate can contribute to the formation of calcium alkali soil from carbonate, which makes it difficult to provide a lot of nutrients for the ancient lake in Es<sub>4</sub>. The relatively low nutrient concentration in the saline waters might lead to the low primary productivity in the saline lake, which appears to be supported by the lighter  $\delta^{13}\text{C}_{\text{OM}}$ , lower Ba-bio values, and Si-bio values for Es<sub>4</sub> samples. Therefore, due to the lack of nutrients from the river, the abundance of plankton (e.g., Bohaidina) may be limited during the period of Es<sub>4</sub>. Increased preservation (relatively stable stratified water conditions) should be responsible for the formation of the potential source rock in Es<sub>4</sub>.

During Es<sub>3</sub>'s deposition, the intense activity of the border fault and rapid subsidence resulted in a deep, fresh water lake and generally regressional or aggradational basin fill (Figure 14B). As the climate became warmer and wetter, the supply of water and sediment increased largely. High water inflow decreased the salinity of water and only unstable temperature stratification can occur in water body (Figure 14B). Therefore, the distribution area of euxinic bottom water is limited due to the relatively deep and unstable temperature stratification, as indicated by the lower Sr/Ba, V/Cr, and V/Sc. Strong physical weathering and chemical weathering under a humid climate increased dissolved inorganic carbon and nitrate of nutrient elements into the lake, which promoted high primary productivity evidenced by relatively high  $^{13}\text{C}$  enrichment in the organic matter of the Es<sub>3</sub> rock. In the freshwater lake, the dinoflagellates Bohaidina and Parabohaidina thrived, as evidenced by the high 4-methylsterane indices, and freshwater microalgae and chlorophyll-containing phytoplankton might also be important members of the community. In brief, the high primary productivity was the main factor accounting for the enrichment of organic matter during the deposition of Es<sub>3</sub>.

In summary, changes in tectonic subsidence and climate during the synrift evolution of Langgu sag caused changes in the hydrological status and water chemistry of the lake, which induced changes in the redox environment and primary productivity. The synergetic evolution of environments and organisms in the lake systems accounted for the deposition of the two source rock intervals with different hydrocarbon generating potentials.

## CONCLUSION

This study presents the geochemical characteristics of the source rocks in the Langgu hydrocarbon-generating sag in the Jizhong subbasin, and the conclusions can be outlined as follows:

(1) Low to medium S<sub>2</sub> and TOC values indicate that the Es<sub>4</sub> and Es<sub>3</sub> source rocks are of poor to fair quality in the Langgu sag in the Jizhong depression.

(2) The distribution and relative concentrations of minerals and elements reveal that the Es<sub>4</sub> source rock was deposited in relatively hydrologically closed conditions under an arid climate. Higher Sr/Ba and V/Sc values suggest high paleosalinity and enhanced reducing environments during Es<sub>4</sub>'s deposition, which provide relatively increased preservation conditions. In comparison, the paleoclimate is more humid, accompanied by enhanced chemical weathering in the deposition of Es<sub>3</sub> source rock, which is evidenced by overall high values of CIA, Q/F, and Al/Ti ratios. The sedimentary environments of Es<sub>3</sub> are characterized by relatively lower paleosalinity and less reducing conditions as a result of this climate.

(3) The crossplot of HI versus  $\Delta\delta^{13}\text{C}_{\text{carb-OM}}$  indicates that enhanced preservation and promoted primary productivity are the main factors in the accumulation of organic matter during the deposition of Es<sub>4</sub> and Es<sub>3</sub> in the Langgu sag, respectively. Nevertheless, the low to medium hydrocarbon-generating potential of Es mudstone indicates that dilution played a significant role in the formation of high-quality source rock. The Es source rock of limited petroleum potential in the Langgu sag could be ascribed to dilution associated with high sedimentation rates in the rift sequences.

## DATA AVAILABILITY STATEMENT

The original contributions presented in the study are included in the article/Supplementary Files; further inquiries can be directed to the corresponding author.

## AUTHOR CONTRIBUTIONS

YC is responsible for the preparation, creation, and/or presentation of the published work, specifically for writing the initial draft (including substantive translation). HZ suggests the ideas, formulation or evolution of overarching research goals and aims, and then preparation, creation, and/or presentation of the published work by those from the original research group, specifically critical review, commentary, or revision including pre- or postpublication stages. FD helps manage activities to annotate (produce metadata), scrub data, and maintain research data.

## FUNDING

This study was financially supported by the National Natural Science Foundation of China, China (42172152) and the National Science & Technology Specific Project, China (No. 2016ZX05024-003-008).

## REFERENCES

- Akul'shina, E. P. (1976). "Methods for Determining Weathering Conditions, Sedimentation and Post-sedimentary Transformations According to Clay Minerals," in *Glinistye Mineraly Kak Pokazatel Litogeneza (Clay Minerals as Indicators of Rock Forming Conditions)*. Editor E. P. Akul'shina (Novosibirsk: Nauka), 9–37. (in Russian).
- Algeo, T. J., and Tribouillard, N. (2009). Environmental Analysis of Paleocyanographic Systems Based on Molybdenum-Uranium Covariation. *Chem. Geol.* 268, 211–225. doi:10.1016/j.chemgeo.2009.09.001
- Allen, M. B., Macdonald, D. I. M., Xun, Z., Vincent, S. J., and Broutet-Menzies, C. (1997). Early Cenozoic Two-phase Extension and Late Cenozoic Thermal Subsidence and Inversion of the Bohai Basin, Northern China. *Mar. Pet. Geol.* 14, 951–972. doi:10.1016/S0264-8172(97)00027-5
- Bohacs, K. M., Carroll, A. R., Neal, J. E., and Mankiewicz, P. J. (2000). "Lake-basin Type, Source Potential, and Hydrocarbon Character: an Integrated Sequence-Stratigraphic-Geochemical Framework," in *Lake Basins through Space and Time: AAPG Studies in Geology*, 46, 3–34.
- Bohacs, K. M., Grabowski, G. J., Jr, Carroll, A. R., Mankiewicz, P. J., Miskellgerhardt, K. J., Schwalbach, J. R., et al. (2005). "Production, Destruction, and Dilution-The Many Paths to Source-Rock Development," in *Deposition of Organic-Carbon-Rich Sediments: Models, Mechanisms, and Consequences* (SEPM Special Publication), 82, 61–101. doi:10.2110/pec.05.82.0061
- Bustin, R. M., and Chonchawalit, A. (1997). Petroleum Source Rock Potential and Evolution of Tertiary Strata, Pattani Basin, Gulf of Thailand. *Bulletin* 81 (1997), 2000–2023. doi:10.1306/3B05C708-172A-11D7-8645000102C1865D
- Cao, J., Wu, M., Chen, Y., Hu, K., Bian, L., Wang, L., et al. (2012). Trace and Rare Earth Element Geochemistry of Jurassic Mudstones in the Northern Qaidam Basin, Northwest China. *Geochemistry* 72, 245–252. doi:10.1016/j.chemer.2011.12.002
- Cao, Y., Wang, Q., Zou, H., Diao, F., Lin, J., Zhang, J., et al. (2017). Genesis Types and Distribution Laws of Crude Oil in Langgu Sag. *Acta Pet. Sin.* 38, 1263–1274. doi:10.7623/syxb201711005
- Cao, Y., Song, H., Algeo, T. J., Chu, D., Du, Y., Tian, L., et al. (2019). Chemical Weathering during the Permian-Triassic Transition Recorded in Terrestrial and Marine Successions. *Palaeogeogr. Palaeoclimatol. Palaeoecol.* 519, 166–177. doi:10.1016/j.palaeo.2018.06.012
- Carroll, A. R., and Bohacs, K. M. (1999). Stratigraphic Classification of Ancient Lakes: Balancing Tectonic and Climatic Controls. *Geology* 27, 99–102. doi:10.1130/0091-7613(1999)027<0099:scoalb>2.3.co;2
- Carroll, A. R., and Bohacs, K. M. (2001). Lake-Type Controls on Petroleum Source Rock Potential in Nonmarine Basins. *Bulletin* 85, 1033–1053. doi:10.1306/8626CA5F-173B-11D7-8645000102C1865D
- Chen, J., Bi, Y., Zhang, J., and Li, S. (1996). Oil-Source Correlation in the Fulin Basin, Shengli Petroleum Province, East China. *Org. Geochem.* 24, 931–940. doi:10.1016/S0146-6380(96)00049-6
- Dahl, T. W., Chappaz, A., Fitts, J. P., and Lyons, T. W. (2013). Molybdenum Reduction in a Sulfidic Lake: Evidence from X-Ray Absorption Fine-Structure Spectroscopy and Implications for the Mo Paleoproxy. *Geochim. Cosmochim. Acta* 103, 213–231. doi:10.1016/j.gca.2012.10.058
- Dettman, D. L., Fang, X., Garzzone, C. N., and Li, J. (2003). Uplift-Driven Climate Change at 12 Ma: A Long  $\delta^{18}\text{O}$  Record From the NE Margin of the Tibetan plateau. *Earth Planet. Sci. Lett.* 214, 267–277. doi:10.1016/S0012-821X(03)00383-2
- Diao, F., Zou, H., Hao, F., Jin, F., Sun, Y., Luo, Q., et al. (2014). Characteristics and Depositional Models of Source Rocks in Langgu Sag, Bohai Bay Basin. *Oil Gas Geol.* 35, 326–335. doi:10.11781/syysdz201404479
- Drummond, C. N., Wilkinson, B. H., Lohmann, K. C., and Smith, G. R. (1993). Effect of Regional Topography and Hydrology on the Lacustrine Isotopic Record of Miocene Paleoclimate in the Rocky Mountains. *Palaeogeogr. Palaeoclimatol. Palaeoecol.* 101, 67–79. doi:10.1016/0031-0182(93)90152-9
- Dymond, J., Suess, E., and Lyle, M. (1992). Barium in Deep-Sea Sediment: A Geochemical Proxy for Paleoproductivity. *Paleoceanography* 7, 163–181. doi:10.1029/92pa00181
- Elderfield, H., Upstill-Goddard, R., and Sholkovitz, E. R. (1990). The Rare Earth Elements in Rivers, Estuaries, and Coastal Seas and Their Significance to the Composition of Ocean Waters. *Geochim. Cosmochim. Acta* 54, 971–991. doi:10.1016/0016-7037(90)90432-K
- Espitalié, J., Laporte, J. L., Madec, M., Marquis, F., Leplat, P., Paulet, J., et al. (1977). Méthode Rapide de Caractérisation des Roches mères, de leur Potentiel Pétrolier et de leur Degré d'évolution. *Rev. Inst. Fr. Pét.* 32, 23–42. doi:10.2516/ogst:1977002
- Fontes, J.-C., Gasse, F., and Gibert, E. (1996). Holocene Environmental Changes in Lake Bangong Basin (Western Tibet). Part 1: Chronology and Stable Isotopes of Carbonates of a Holocene Lacustrine Core. *Palaeogeogr. Palaeoclimatol. Palaeoecol.* 120, 25–47. doi:10.1016/0031-0182(95)00032-1
- Fu, J., Sheng, G., Xu, J., Eglinton, G., Gowar, A. P., Jia, R., et al. (1990). Application of Biological Markers in the Assessment of Paleoenvironments of Chinese Non-marine Sediments. *Org. Geochem.* 16, 769–779. doi:10.1016/0146-6380(90)90116-H
- Goldberg, K., and Humayun, M. (2010). The Applicability of the Chemical Index of Alteration as a Paleoclimatic Indicator: An Example from the Permian of the Paraná Basin, Brazil. *Palaeogeogr. Palaeoclimatol. Palaeoecol.* 293, 175–183. doi:10.1016/j.palaeo.2010.05.015
- Goldstein, S. J., and Jacobsen, S. B. (1987). The Nd and Sr Isotopic Systematics of River-Water Dissolved Material: Implications for the Sources of Nd and Sr in Seawater. *Chem. Geol. Isot. Geosci. Sect.* 66, 245–272. doi:10.1016/0168-9622(87)90045-5
- Gonçalves, F. T. T. (2002). Organic and Isotope Geochemistry of the Early Cretaceous Rift Sequence in the Camamu Basin, Brazil: Paleolimnological Inferences and Source Rock Models. *Org. Geochem.* 33, 67–80. doi:10.1016/S0146-6380(01)00128-0
- Haberzettl, T., Kück, B., Wulf, S., Anselmetti, F., Ariztegui, D., Corbella, H., et al. (2008). Hydrological Variability in Southeastern Patagonia and Explosive Volcanic Activity in the Southern Andean Cordillera during Oxygen Isotope Stage 3 and the Holocene Inferred from Lake Sediments of Laguna Potrok Aike, Argentina. *Palaeogeogr. Palaeoclimatol. Palaeoecol.* 259, 213–229. doi:10.1016/j.palaeo.2007.10.008
- Hanson, A. D., Ritts, B. D., Zinniker, D., Moldowan, J. M., and Biffi, U. (2001). Upper Oligocene Lacustrine Source Rocks and Petroleum Systems of the Northern Qaidam Basin, Northwest China. *Bulletin* 85, 601–619. doi:10.1306/8626C95B-173B-11D7-8645000102C1865D
- Hao, F., Zhou, X., Zhu, Y., Zou, H., Bao, X., and Kong, Q. (2009a). Mechanisms of Petroleum Accumulation in the Bozhong Sub-basin, Bohai Bay Basin, China. Part 1. *Mar. Pet. Geol.* 26, 1528–1542. doi:10.1016/j.marpetgeo.2008.09.005
- Hao, F., Zhou, X., Zhu, Y., Bao, X., and Yang, Y. (2009b). Charging of the Neogene Penglai 19-3 Field, Bohai Bay Basin, China: Oil Accumulation in a Young Trap in an Active Fault Zone. *Bulletin* 93, 155–179. doi:10.1306/09080808092
- Hao, F., Zhou, X., Zhu, Y., and Yang, Y. (2009c). Mechanisms for Oil Depletion and Enrichment on the Shijiutuo Uplift, Bohai Bay Basin, China. *Bulletin* 93, 1015–1037. doi:10.1306/04140908156
- Hao, F., Zhou, X., Zhu, Y., Zou, H., and Yang, Y. (2010). Charging of Oil Fields Surrounding the Shaleitian Uplift from Multiple Source Rock Intervals and Generative Kitchens, Bohai Bay Basin, China. *Mar. Pet. Geol.* 27, 1910–1926. doi:10.1016/j.marpetgeo.2010.07.005
- Hao, F., Zhou, X., Zhu, Y., and Yang, Y. (2011). Lacustrine Source Rock Deposition in Response to Co-evolution of Environments and Organisms Controlled by Tectonic Subsidence and Climate, Bohai Bay Basin, China. *Org. Geochem.* 42, 323–339. doi:10.1016/j.orggeochem.2011.01.010
- Harris, N. B., Freeman, K. H., Pancost, R. D., White, T. S., and Mitchell, G. D. (2004). The Character and Origin of Lacustrine Source Rocks in the Lower Cretaceous Synrift Section, Congo Basin, West Africa. *Bulletin* 88, 1163–1184. doi:10.1306/02260403069
- Harris, N. B. (2000). Evolution of the Congo Rift Basin, West Africa: an Inorganic Geochemical Record in Lacustrine Shales. *Basin Res.* 12, 425–445. doi:10.1111/j.1365-2117.2000.00129.x
- Haskin, L. A., Wildeman, T. R., and Haskin, M. A. (1968). An Accurate Procedure for the Determination of the Rare Earths by Neutron Activation. *J. Radioanal. Chem.* 1, 337–348. doi:10.1007/bf02513689
- Hollander, D. J., and McKenzie, J. A. (1991). CO<sub>2</sub> Control on Carbon-Isotope Fractionation during Aqueous Photosynthesis: A Paleo-pCO<sub>2</sub> Barometer. *Geology* 19, 929–932. doi:10.1130/0091-7613(1991)019<0929:ccocif>2.3.co;2
- Hollander, D. J., McKenzie, J. A., and Haven, H. L. T. (1992). A 200 Year Sedimentary Record of Progressive Eutrophication in Lake Greifen

- (Switzerland): Implications for the Origin of Organic-Carbon-Rich Sediments. *Geology* 20, 825–828. doi:10.1130/0091-7613(1992)020<0825:AYSROP>2.3.CO;2
- Hollander, D. J., McKenzie, J. A., Hsu, K. J., and Huc, A. Y. (1993). Application of an Eutrophic Lake Model to the Origin of Ancient Organic-Carbon-Rich Sediments. *Glob. Biogeochem. Cycles* 7, 157–179. doi:10.1029/92gb02831
- Hou, D., Zhang, S., Xiao, J., Zhang, L., Zhang, H., Cheng, S., et al. (2008). The Excellent Source Rocks and Accumulation of Stratigraphic and Lithologic Traps in the Jiyang Depression, Bohai Bay Basin, China. *Earth Sci. Front.* 15, 137–146. doi:10.1016/s1872-5791(08)60041-x
- Ibach, L. E. J. (1982). Relationship between Sedimentation Rate and Total Organic Carbon Content in Ancient Marine Sediments. *Bulletin* 66, 170–188. doi:10.1306/03B59A5D-16D1-11D7-8645000102C1865D
- Jaraula, C. M. B., Siringan, F. P., Klingel, R., Sato, H., and Yokoyama, Y. (2014). Records and causes of Holocene Salinity Shifts in Laguna de Bay, Philippines. *Quat. Int.* 349, 207–220. doi:10.1016/j.quaint.2014.08.048
- Jones, B., and Manning, D. A. C. (1994). Comparison of Geochemical Indices Used for the Interpretation of Palaeoredox Conditions in Ancient Mudstones. *Chem. Geol.* 111, 111–129. doi:10.1016/0009-2541(94)90085-X
- Jones, R. W. (1987). “Organic Facies,” in *Advances in Petroleum Geochemistry*. Editors J. Brooks and D. Welte (New York: Academic Press), 1–90.
- Kamp, P. C. V. D. (2010). Arkose, Subarkose, Quartz Sand, and Associated Muds Derived from Felsic Plutonic Rocks in Glacial to Tropical Humid Climates. *J. Sediment. Res.* 80, 895–918. doi:10.2110/jsr.2010.081
- Katz, B. J. (2001). Lacustrine Basin Hydrocarbon Exploration—Current Thoughts. *J. Paleolimnol.* 26, 161–179. doi:10.1023/A:1011173805661
- Katz, B. J. (2005). *Controlling Factors on Source Rock Development - A Review of Productivity, Preservation and Sedimentation Rate*. Tulsa: SEPM Society for Sedimentary Geology, 7–16. doi:10.2110/pec.05.82.0001
- Keym, M., Dieckmann, V., Horsfield, B., Erdmann, M., Galimberti, R., Kua, L.-C., et al. (2006). Source Rock Heterogeneity of the Upper Jurassic Draupne Formation, North Viking Graben, and its Relevance to Petroleum Generation Studies. *Org. Geochem.* 37, 220–243. doi:10.1016/j.orggeochem.2005.08.023
- Kiipli, E., Kiipli, T., Kallaste, T., and Siir, S. (2012). Al<sub>2</sub>O<sub>3</sub>/TiO<sub>2</sub> Ratio of the Clay Fraction of Late Ordovician-Silurian Carbonate Rocks as an Indicator of Paleoclimate of the Fennoscandian Shield. *Palaeogeogr. Palaeoclimatol. Palaeoecol.* 365–366, 312–320. doi:10.1016/j.palaeo.2012.10.001
- Kimura, H., and Watanabe, Y. (2001). Oceanic Anoxia at the Precambrian-Cambrian Boundary. *Geology* 29, 9952–9998. doi:10.1130/0091-7613(2001)029<0995:oaatpc>2.0.co;2
- Lamb, A. L., Wilson, G. P., and Leng, M. J. (2006). A Review of Coastal Palaeoclimate and Relative Sea-Level Reconstructions Using  $\delta^{13}\text{C}$  and C/N Ratios in Organic Material. *Earth-Sci. Rev.* 75, 29–57. doi:10.1016/j.earscirev.2005.10.003
- Li, X., and Liu, W. (2014). Water Salinity and Productivity Recorded by Ostracod Assemblages and Their Carbon Isotopes since the Early Holocene at Lake Qinghai on the Northeastern Qinghai-Tibet Plateau, China. *Palaeogeogr. Palaeoclimatol. Palaeoecol.* 407, 25–33. doi:10.1016/j.palaeo.2014.04.017
- Li, D., Li, R., Li, R., Zhu, Z., Wu, X., Zhao, B., et al. (2017). Rare Earth Elements Geochemistry Characteristics and Their Geological Implications of Lacustrine Oil Shale From Chang 7 Oil Layer in Southern Ordos Basin, China. *Geol. J.* 52, 119–131. doi:10.1002/gi.2980
- Liu, C., Zhao, J., Ma, Y., Wang, J., Xiong, L., Chen, J., et al. (2014). The Advances and Problems in the Study of the Characteristics and Formation of Hydrocarbon-Rich Sag. *Earth Sci. Front.* 21, 75–88.
- Liu, B., Bechtel, A., Sachsenhofer, R. F., Gross, D., Gratzner, R., and Chen, X. (2017). Depositional Environment of Oil Shale within the Second Member of Permian Lucaogou Formation in the Santanghu Basin, Northwest China. *Int. J. Coal Geol.* 175, 10–25. doi:10.1016/j.coal.2017.03.011
- Liu, B., Bechtel, A., Gross, D., Fu, X., Li, X., and Sachsenhofer, R. F. (2018a). Middle Permian Environmental Changes and Shale Oil Potential Evidenced by High-Resolution Organic Petrology, Geochemistry and Mineral Composition of the Sediments in the Santanghu Basin, Northwest China. *Int. J. Coal Geol.* 185, 119–137. doi:10.1016/j.coal.2017.11.015
- Liu, B., Yan, D., Fu, X., Lv, Y., Gong, L., and Wang, S. (2018b). Investigation of Geochemical Characteristics of Hydrocarbon Gas and its Implications for Late Miocene Transpressional Strength—A study in the Fangzheng Basin, Northeast China. *Interpretation* 6, 83–96. doi:10.1190/int-2017-0092.1
- Makeen, Y. M., Hakimi, M. H., and Abdullah, W. H. (2015). The Origin, Type and Preservation of Organic Matter of the Barremian-Aptian Organic-Rich Shales in the Muglad Basin, Southern Sudan, and their Relation to Paleoenvironmental and Paleoclimate Conditions. *Mar. Pet. Geol.* 65, 187–197. doi:10.1016/j.marpetgeo.2015.03.003
- McLennan, S. M. (1993). Weathering and Global Denudation. *J. Geol.* 101, 295–303. doi:10.1086/648222
- Meyers, P. A. (1997). Organic Geochemical Proxies of Paleoceanographic, Paleolimnologic, and Paleoclimatic Processes. *Org. Geochem.* 27, 213–250. doi:10.1016/S0146-6380(97)00049-1
- Nesbitt, H. W., and Markovics, G. (1997). Weathering of Granodioritic Crust, Long-Term Storage of Elements in Weathering Profiles, and Petrogenesis of Siliciclastic Sediments. *Geochim. Cosmochim. Acta* 61, 1653–1670. doi:10.1016/S0016-7037(97)00031-8
- Neuhuber, S., Gier, S., Hohenegger, J., Wolfgring, E., Spötl, C., Strauss, P., et al. (2016). Palaeoenvironmental Changes in the Northwestern Tethys during the Late Campanian Radotruncana calcarata Zone: Implications from Stable Isotopes and Geochemistry. *Chem. Geol.* 420, 280–296. doi:10.1016/j.chemgeo.2015.11.023
- Pérez, L., Curtis, J., Brenner, M., Hodell, D., Escobar, J., Lozano, S., et al. (2013). Stable Isotope Values ( $\delta^{18}\text{O}$  &  $\delta^{13}\text{C}$ ) of Multiple Ostracode Species in a Large Neotropical Lake as Indicators of Past Changes in Hydrology. *Quater. Sci. Rev.* 66, 96–111. doi:10.1016/j.quascirev.2012.10.044
- Peters, K. E. (1986). Guidelines for Evaluating Petroleum Source Rock Using Programmed Pyrolysis. *Bulletin* 70, 318–329. doi:10.1306/94885688-1704-11D7-8645000102C1865D
- Powell, W. (2009). Comparison of Geochemical and Distinctive Mineralogical Features Associated with the Kinzers and Burgess Shale formations and their Associated Units. *Palaeogeogr. Palaeoclimatol. Palaeoecol.* 277, 127–140. doi:10.1016/j.palaeo.2009.02.016
- Qi, J., and Yang, Q. (2010). Cenozoic Structural Deformation and Dynamic Processes of the Bohai Bay Basin Province, China. *Mar. Pet. Geol.* 27 (4), 757–771. doi:10.1016/j.marpetgeo.2009.08.012
- Ross, D. J. K., and Bustin, R. M. (2009). Investigating the use of sedimentary geochemical proxies for paleoenvironment interpretation of thermally mature organic-rich strata: Examples from the Devonian-Mississippian shales, Western Canadian Sedimentary Basin. *Chem. Geol.* 260, 1–19. doi:10.1016/j.chemgeo.2008.10.027
- Schoepfer, S. D., Shen, J., Wei, H., Tyson, R. V., Ingall, E., and Algeo, T. J. (2015). Total Organic Carbon, Organic Phosphorus, and Biogenic Barium Fluxes as Proxies for Paleomarine Productivity. *Earth-Sci. Rev.* 149, 23–52. doi:10.1016/j.earscirev.2014.08.017
- Shaw, T. J., Gieskes, J. M., and Jahnke, R. A. (1990). Early Diagenesis in Differing Depositional Environments: The Response of Transition Metals in Pore Water. *Geochim. Cosmochim. Acta* 54, 1233–1246. doi:10.1016/0016-7037(90)90149-F
- Sheldon, N. D., and Tabor, N. J. (2009). Quantitative Paleoenvironmental and Paleoclimatic Reconstruction Using Paleosols. *Earth-Sci. Rev.* 95, 1–52. doi:10.1016/j.earscirev.2009.03.004
- Sinha, R., Smykatz-Kloss, W., Stüben, D., Harrison, S. P., Berner, Z., and Kramar, U. (2006). Late Quaternary Palaeoclimatic Reconstruction from the Lacustrine Sediments of the Sambhar Playa Core, Thar Desert Margin, India. *Palaeogeogr. Palaeoclimatol. Palaeoecol.* 233, 252–270. doi:10.1016/j.palaeo.2005.09.012
- Sinninghe, D. J., Kenig, F., Koopmans, M. P., Köster, J., Schouten, S., Hayes, J. M., et al. (1995). Evidence for Gammacerane as an Indicator of Water Column Stratification. *Geochim. Cosmochim. Acta* 59, 1895–1900. doi:10.1016/0016-7037(95)00073-9
- Song, R., Zhang, S., and Li, T. (2006). Research on the Hydrocarbon Distribution Controlled by Daxing Fault in Langgu Sag. *Nat. Gas Ind.* 26 (08), 30–33 (in Chinese with English abstract).
- Talbot, M. R. (1990). A Review of the Palaeohydrological Interpretation of Carbon and Oxygen Isotopic Ratios in Primary Lacustrine Carbonates. *Chem. Geol. Isot. Geosci. Sect.* 80, 261–279. doi:10.1016/0168-9622(90)90009-2
- Tribouillard, N., Algeo, T. J., Lyons, T., and Riboulleau, A. (2006). Trace Metals as Paleoredox and Paleoproductivity Proxies: An Update. *Chem. Geol.* 232, 12–32. doi:10.1016/j.chemgeo.2006.02.012
- Tyson, R. V. (2001). Sedimentation Rate, Dilution, Preservation and Total Organic Carbon: Some Results of a Modelling Study. *Org. Geochem.* 32, 333–339. doi:10.1016/S0146-6380(00)00161-3

- Valero Garcés, B. L., Kelts, K., and Ito, E. (1995). Oxygen and Carbon Isotope Trends and Sedimentological Evolution of a Meromictic and Saline Lacustrine System: The Holocene Medicine Lake Basin, North American Great Plains, USA. *Palaeogeogr. Palaeoclimatol. Palaeoecol.* 117, 253–278. doi:10.1016/0031-0182(94)00136-V
- Vosoughi Moradi, A., Sari, A., and Akkaya, P. (2016). Geochemistry of the Miocene oil shale (Hançili Formation) in the Çankırı-Çorum Basin, Central Turkey: Implications for Paleoclimate conditions, Source-Area Weathering, Provenance and Tectonic Setting. *Sediment. Geol.* 341, 289–303. doi:10.1016/j.sedgeo.2016.05.002
- Wang, G., Wang, T.-G., Simoneit, B. R. T., Zhang, L., and Zhang, X. (2010). Sulfur Rich Petroleum Derived from Lacustrine Carbonate Source Rocks in Bohai Bay Basin, East China. *Org. Geochem.* 41, 340–354. doi:10.1016/j.orggeochem.2009.12.010
- Wang, Q., Hao, F., Xu, C., Wang, Y., and Zou, H. (2015). Geochemical Characterization of QHD29 Oils on the Eastern Margin of Shijiutuo Uplift, Bohai Sea, China: Insights from Biomarker and Stable Carbon Isotope Analysis. *Mar. Pet. Geol.* 64, 266–275. doi:10.1016/j.marpetgeo.2015.03.010
- Wang, P., Du, Y., Yu, W., Algeo, T. J., Zhou, Q., Xu, Y., et al. (2020). The Chemical Index of Alteration (CIA) as a Proxy for Climate Change During Glacial-Interglacial Transitions In Earth History. *Earth-Sci. Rev.* 201, 103032. doi:10.1016/j.earscirev.2019.103032
- Wang, Q., Hao, F., Xu, C., and Zou, H. (2020). Paleolimnological Environments and the Formation of High Quality Source Rocks in the Bohai Bay Basin: An Integrated Geochemical Study of Biomarkers, Stable Carbon and Oxygen Isotopes, and Trace Elements. *J. Pet. Sci. Eng.* 195, 107753. doi:10.1016/j.petrol.2020.107753
- Warrier, A. K., and Shankar, R. (2009). Geochemical Evidence for the Use of Magnetic Susceptibility as a Paleorainfall Proxy in the Tropics. *Chem. Geol.* 265, 553–562. doi:10.1016/j.chemgeo.2009.05.023
- Wedepohl, K. H. (1971). Environmental Influences on the Chemical Composition of Shales and Clays. *Phys. Chem. Earth* 8, 307–333. doi:10.1016/0079-1946(71)90020-6
- Wei, W., and Algeo, T. J. (2020). Elemental Proxies for Paleosalinity Analysis of Ancient Shales and Mudrocks. *Geochim. Cosmochim. Acta* 287, 341–366. doi:10.1016/j.gca.2019.06.034
- Wei, G., Liu, Y., Li, X., Shao, L., and Fang, D. (2004). Major and Trace Element Variations of the Sediments at ODP Site 1144, South China Sea, during the last 230 ka and their Paleoclimate Implications. *Palaeogeogr. Palaeoclimatol. Palaeoecol.* 212, 331–342. doi:10.1016/s0031-0182(04)00329-3
- Yin, J., Wang, Q., Hao, F., Guo, L., and Zou, H. (2018). Palaeoenvironmental Reconstruction of Lacustrine Source Rocks in the Lower 1st Member of the Shahejie Formation in the Raoyang Sag and The Baxian Sag, Bohai Bay Basin, Eastern China. *Palaeogeogr. Palaeoclimatol. Palaeoecol.* 495, 87–104. doi:10.1016/j.palaeo.2017.12.032
- Yin, J., Xu, C., Hao, F., Wang, Q., Miao, Q., Wang, Z., et al. (2020). Controls on Organic Matter Enrichment in Source Rocks of the Shahejie Formation in the Southwestern Bohong Sag, Bohai Bay Basin, China. *Palaeogeogr. Palaeoclimatol. Palaeoecol.* 560, 110026. doi:10.1016/j.palaeo.2020.110026
- Zakir Hossain, H. M., Sampei, Y., and Roser, B. P. (2009). Characterization of Organic Matter and Depositional Environment of Tertiary Mudstones from the Sylhet Basin, Bangladesh. *Org. Geochem.* 40, 743–754. doi:10.1016/j.orggeochem.2009.04.009
- Zhang, W., Cui, Z., Han, C., Guo, Y., Wang, H., Li, L., et al. (2008). Sedimentary Structural Characteristics and Hydrocarbon Distributed Rules of Jizhong Depression. *Acta Geol. Sin.* 82 (8), 1103–1112. (in Chinese with English abstract).
- Zhao, Z., Zhao, J., Wang, H., Liao, J., and Liu, C. (2007). Distribution Characteristics and Applications of Trace Elements in Junggar Basin. *Nat. Gas Explor. Dev.* 30 (2), 30–32. (in Chinese with English abstract).
- Zhao, X., Jin, F., Wang, Q., and Bai, G. (2015a). Buried-Hill Play, Jizhong Subbasin, Bohai Bay Basin: A review and Future Prospectivity. *Bulletin* 99, 1–26. doi:10.1306/07171413176
- Zhao, X., Liu, C., Jin, F., Jin, Q., and Zhang, Y. (2015b). Petroleum Genetic Types and Oil-Gas sources of Deep Reservoirs in Baxian Depression, Northeast China. *J. Pet. Sci. Eng.* 134, 105–113. doi:10.1016/j.petrol.2015.07.023
- Zhao, X., Jiang, Y., Jin, F., Liu, H., Yang, D., Wang, X., et al. (2017). Hydrocarbon Accumulation Mechanism and Model of Sub-Sags in Hydrocarbon-Rich Sag: a Case Study of Raoyang Sag in Jizhong Depression. *Acta Pet. Sin.* 38, 67–76. (in Chinese with English abstract). doi:10.7623/syxb201701007
- Zhou, L., Algeo, T. J., Shen, J., Hu, Z., Gong, H., Xie, S., et al. (2015). Changes in Marine Productivity and Redox Conditions During the Late Ordovician Hirnantian Glaciation. *Palaeogeogr. Palaeoclimatol. Palaeoecol.* 420, 223–234. doi:10.1016/j.palaeo.2014.12.012

**Conflict of Interest:** The authors declare that the research was conducted in the absence of any commercial or financial relationships that could be construed as a potential conflict of interest.

**Publisher's Note:** All claims expressed in this article are solely those of the authors and do not necessarily represent those of their affiliated organizations, or those of the publisher, the editors, and the reviewers. Any product that may be evaluated in this article, or claim that may be made by its manufacturer, is not guaranteed or endorsed by the publisher.

Copyright © 2022 Cao, Diao and Zou. This is an open-access article distributed under the terms of the Creative Commons Attribution License (CC BY). The use, distribution or reproduction in other forums is permitted, provided the original author(s) and the copyright owner(s) are credited and that the original publication in this journal is cited, in accordance with accepted academic practice. No use, distribution or reproduction is permitted which does not comply with these terms.